People's **D**emocratic **R**epublic of **A**lgeria **M**inistry of **H**igher **E**ducation and **S**cientific **R**esearch

University of 20 Aout 1955-Skikda

Faculty of Sciences

Department of Physics

N° : D02P202430M

Master Thesis

Division: Physics

Specialty: Radiation Physics

Thesis entitled:

Structural, optical and electrical characterization of Li-doped CuO thin layers obtained by spray pyrolysis

Presented by:

Boudeffa Asma

Defended on : …./…./…….. before the jury composed of:

K.Khonfais	Professor	University of 20 aout 1955- Skikda	President
R. Daira	MCA	University of 20 aout 1955- Skikda	Supervisor
A.Fekrache	MCB	University of 20 aout 1955- Skikda	Examiner

Academic Year : 2023/2024

Acknowledgments

At first, I express my gratefulness to the Almighty Allah for giving me the strength to complete this research.

I would like to thank my supervisor "Dr. Daira Radouane" for his guidance, encouragement and the countless opportunities he has presented to me over the course of my master: I couldn't have asked for a better supervisor or a nicer person, who has a genuine desire to cultivate creative science, and benefit society through the field in which he excels.

My special thanks goes out to: "Dr Khelili Farid" and the countless others who have helped me along the way.

Asma

Dedication

To everyone who gave us hope and confidence to reach what we want…

To everyone who encouraged us to continue…

To everyone who repeated to us calls for success…

Asma Boudeffa

Résumé :

Dans le présent travail, les propriétés structurales, optiques et électriques des couches minces d'oxyde cuprique dopées au Li (0-6 à 0.%) ont été étudiées. Les films ont été obtenus par pyrolyse par pulvérisation sur des substrats de verre à 350°C. La méthode de diffraction des rayons X, UV-Vis. La spectroscopie et la technique de sonde à quatre points ont été utilisées pour analyser les films. Selon les investigations DRX, il a été constaté que les films poly-cristallins ont des phases monocliniques avec des plans cristallographiques préférés (002) et (-111). L'incorporation du dopage Li dans le film mince CuO a donné des tailles cristallines d'environ 12 nm. Les valeurs estimées de l'écart de bande optique diminuent avec l'augmentation de la concentration de Li de 1,88 à 1,64 eV. Les études par sonde à quatre points ont révélé que la résistivité des films diminuait de 339 à 186 KΩ.cm avec l'augmentation de la concentration en Li.

Mots clés : CuO, Dopage Li, spray en mode discontinu, couche mince.

Abstract:

In the present work, the structural, optical and electrical properties of Li-doped (0-6 at.%) cupric oxide thin films were investigated. The films were obtained by the spray pyrolysis method on glass substrates at 450°C. The X-ray diffraction method, UV-Vis. spectroscopy and the four-point probe technique were used to analyze the films. According the XRD investigations, it was found that the polycrystalline films have monoclinic phases with a preferred (002) and (-111) crystallographic planes. The incorporation of Li doping into the CuO thin film yielded crystallite sizes of approximately 12 nm. The estimated optical band gap values are decreased with increasing Li concentration from 1.88 to 1.64 eV. Four-point probe studies revealed that the resistivity of the films decreased from 339 to 186 KΩ.cm with increasing Li concentration.

Keywords: CuO, Li-doping, Spray pyrolysis, Thin film.

LIST OF TABLES

LIST OF FIGURES

LIST OF ABBREVIATIONS

Symbole	Description
TCO	Transparent conducting oxides
CuO	Copper oxide
PVD	Physical Vapor Deposition
CVD	Chemical Vapor Deposition
MBE	Molecular Beam Epitaxy
PLD	Pulsed Laser Deposition
APCVD	Atmospheric Pressure Chemical Vapor Deposition
LPCVD	Low-Pressure Chemical Vapor Deposition

MOCVD	Metal Organic CVD
PACVD	Plasma Assisted Chemical Vapor Deposition
CBD	Chemical bath deposition
XRD	X- Ray Diffraction
d(hkl)	Inter-Plane Distance of Atoms or Ions or Molecules
n	Order of reflection
$\boldsymbol{\theta}$	Bragg angle
$\boldsymbol{\lambda}$	Photon wavelength
$\boldsymbol{\beta}$= FWHM	Full width at the half maximum of the XRD peak
D	Crystallite size
d	Interplanar spacing
, b, c	Lattice constants
$\boldsymbol{\varepsilon}$	Microstrain
$\boldsymbol{\delta}$	Dislocation density
$\boldsymbol{N_0}$	number of crystallites
t	thickness
UV	Ultraviolet

UV-Vis	Ultraviolet-visible
v	Frequency of photon
h	Planck's constant
hv	Photon Energy
Eg	Gap Energy
$\boldsymbol{\alpha}$	Absorption co-efficient
A	Absorbance
T	Transmittance
R	Reflectance
$\boldsymbol{\rho}$	Electrical resistivity
V	Voltage
I	Current

CONTENTS

INTRODUCTION

Nanomaterials and nanodevices are the most important aspects of nanotechnology with a bright future of real-world applications to serve and monitor humanity's environment. These nanostructure materials are known to derive real benefits from semiconductor metal oxides (TCO). These materials have interesting properties such as chemical stability, electrochemical activity, and ease of synthesis. Metal oxide semiconductors are the indisputable prerequisite for the development of diverse and intelligent materials. These TCOs have attracted much attention not only for basic scientific research, but also for various practical applications for their interesting physical and chemical properties.

Among all these metal oxides, copper oxide (CuO) has gained a leading edge in the most active fields of technological applications. This material shows great attention in different fields to improve new methods easy, inexpensive and effective for scientific research and industries because of its appropriate range of applications. In addition, copper oxide CuO has been a hot topic through progress studies because of its interesting properties as a semiconductor type p with a direct optical gap equal to 1.2 eV, simplicity of preparation, abundant in nature, low cost and non-toxic. This material is considered today as one of the most used in photovoltaics for the manufacture of solar cells, its high solar absorption, its low thermal emission, its good electrical properties and its high carrier concentration. This material is also promising as an electrode material for the next generation of rechargeable lithium

batteries due to its high theoretical capacity, safety and environmental friendliness. It is also widely considered for gas sensor applications. Thus, CuO applications are expected to increase rapidly due to its unique high-quality crystalline phase. Therefore, this material has been studied to be considered a future material, given its encouraging properties in various other applications, including energy materials, supercapacitors, magnetic storage, field emissions, photodetectors, spintronics and superconductors with high TC, photocatalysis, nanofluids and heat transfer applications, biosensors, anticancer and antimicrobial activities and the removal of inorganic pollutants. Based on these considerations, CuO nanostructures also have more attractive magnetic properties.

Experimentally, CuO thin films were prepared using various chemical and physical techniques, including spin coating, immersion coating, sol gel, SILAR, spraying, thermal evaporation, laser ablation, electroplating, chemical vapor deposition and spray pyrolysis. Spray pyrolysis has attracted several researches according to its simplicity, inexpensive and cost-effective technique. The spraying method leads to the formation of good quality films. In fact, the preparation of CuO thin films with this technique shows excellent results in comparison with other techniques.

The objective of this thesis is to prepare thin layers of copper oxide with Li doping by spray technique in discontinuous mode by varying the percentage of doping. We strive to optimize the suitable doping rate in order to obtain good quality CuO films. To do this we have followed the evolution of the electrical and optical properties with the elevation of the doping rate for the understanding of the effect of this parameter on the properties of this material in order to optimize their performances for their uses in technological devices such as solar cells.

Our brief is structured in three chapters as follows:

In the first chapter, we expose the definition, the electrical and optical properties of copper oxide and its applications in solar cells, gas sensors and photocatalysis.

The second chapter presents the different techniques for the development of layers according to the physical (PVD) and chemical (CVD) process. Thus characterization techniques such as: XDR, Raman spectroscopy, four-point technique and UV-Visible spectroscopy.

In the third chapter we will present the evolution of the structural, electrical and optical properties of copper oxide thin films CuO with the increase of the percentage of doping by

Li, these films are deposited on a glass substrate heated to a temperature of $\mathbf{350^0}$C by the spray method in batch mode using the 0.1 M copper chloride solution and as a source of dopant we used iron chloride.

CHAPTER

1

BASICS ON THIN FILMS

This chapter offers a fresh perspective on thin films. It includes a description of thin films and an overview of their applications.

1.1 Thin film

1.1.1 Definition of thin film

Thin film technology is simultaneously one of the oldest arts and one of the newest research studies [1]. Thin films and nanostructured coatings are essential to clean technology because they allow to do a lot with a little amount of masse[2]. They are generally used to improve the surface properties of solids. Thin films principle is a substance deposited in another substance called a substrate [1]. It can be prepared as semiconductors, resistors, conductors and insulator, all preparation types are widely used in many industrial applications [3]. A thin film may also be defined as a layer of material with a thickness ranging from one nanometer to several micrometers. Also it's well known that layer of material with one

dimension is much smaller than the other[4].

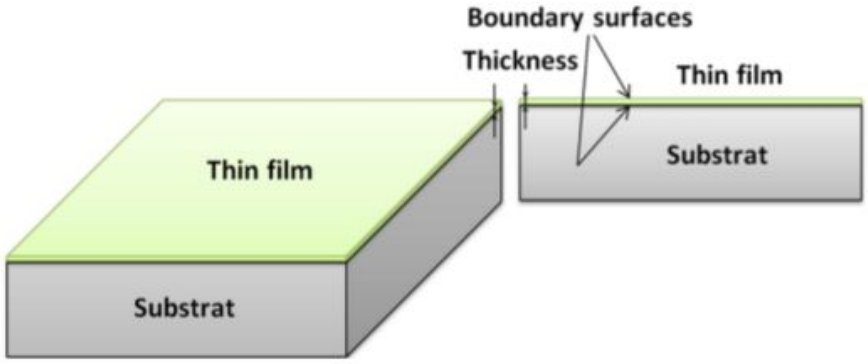

Figure 1.1: Schematic of thin film deposited on a glass substrate.

1.1.2 Steps to formation of thin films

In the synthesis process of thin films, the coating material must pass through a conductive medium and come into direct contact with the substrate to form a thin film on a solid surface (substrate). A portion of the coating particles adheres or chemically reacts with the substrate when they land on it. The particles can be either atoms, molecules, ions, or molecular fragments coming from molecules that have been ionized or fragmented. Nevertheless, all thin film deposition techniques consist of four consecutive phases :

Source : The fundamental constituent of the thin film to be generated may initially consist of a solid, a liquid, or a gas [5].

Transport : The homogeneity of the flow of species throughout the transport stage onto the substrate surface is a crucial property to preserve but it is influenced by several parameters that are contingented by the medium in which the transport occurs.

Deposition : The third stage in the fabrication of thin films involves the application of a layer onto the surface of the substrate. This phase encompasses the processes of nucleation and fusion. The deposition process is influenced by various factors, including the source and transport mechanisms as well as the primary surface conditions of the substrate. These surface conditions encompass characteristics such as surface roughness, contamination levels and other relevant factors. Additionally, the bonding coefficient of the material arriving on the substrate surface and the temperature of the substrate also play a significant role in

determining the deposition behavior [6].

Analysis : The final stage of the production process involves the examination and analysis of the thus-deposited film [7].

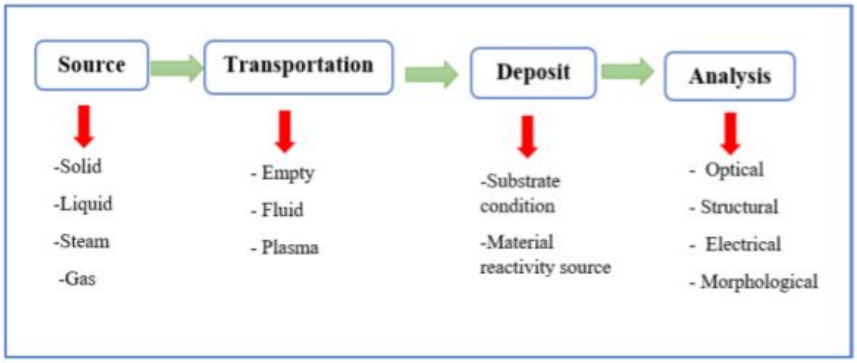

Figure 1.2: Schematic diagram of the steps of the thin film fabrication process.

1.1.3 Classification of growth patterns

In a simple approach, the growth of thin films on a substrate is classified into three categories schematically illustrated (Figure I.11) [[8],[9]].

Island growth (Volmer-Weber mode)

In this mode of growth, small clusters nucleate directly on the surface the substrate and grow in islands on it. This growth will take place when atoms or molecules that arrive on the surface of the substrate are more likely to bond between them than with the substrate. A typical case this growth is that metallic films on insulating substrates.

Layered growth (Franck-Van der Merwe mode)

This mode of growth takes place when the adatom-substrate interaction is very strong. The first atoms which arrive on the surface the substrate condense and form a monolayer covering the entire surface: we then have a growth two-dimensional of nuclei to form a layer, and then growth layer by layer.

Mixed growth (Stranski-Krastanov mode)

This mode of growth is an intermediate case: growth is first two-dimensional to form the first layer(s); however, as the energy of adatom-substrate interaction gradually decreases, the growth tends to become three-dimensional with the formation of islands.

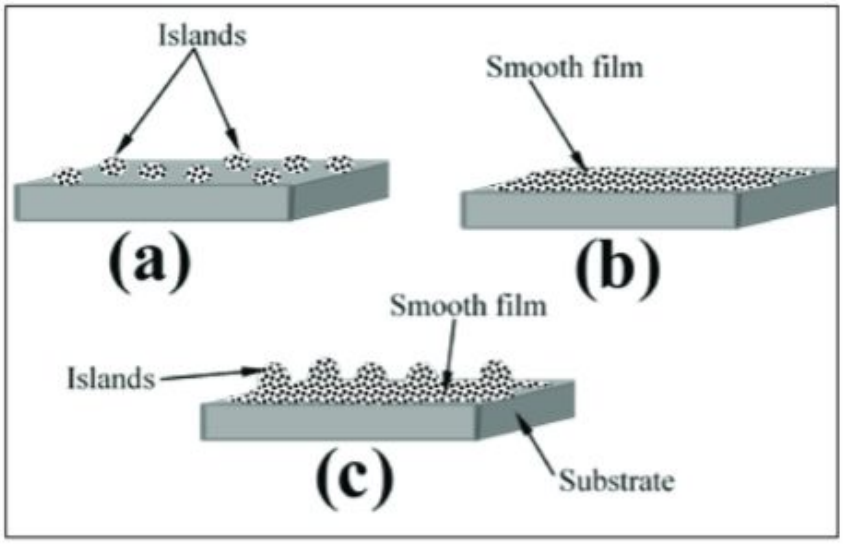

Figure 1.3: Basic Modes of thin film growth: (a) island (b) layer-by-layer and (c) layer plus island.

1.1.4 Thin film growth mechanism

All thin film processes are done in three stages:

- The production of appropriate ionic, molecular, atomic species.
- The transport of these species to the substrate.
- Condensation on this same substrate is done either directly or through a chemical or electrochemical reaction in order to form the solid deposit; this step often goes through three phases: nucleation, coalescence then growth.

a) **Nucleation** It is the phenomenon that accompanies changes in the state of matter and which consists in the appearance, within a given medium, of transformation points from which a new physical or chemical structure develops.
The entire surface of it, in this state, they interact with each other and form what are

called "clusters". These "clusters" also called nuclei, are unstable and tend to subside. Under certain deposit conditions, they collide with other adsorbed species and start to grow. After reaching a critical size, these clusters become thermodynamically stable and the nucleation barrier is crossed. The nucleation stage is shown in figure I.4.

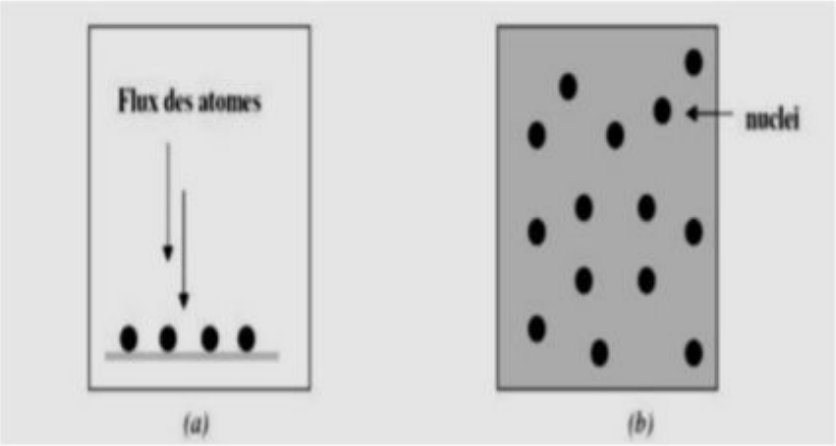

Figure 1.4: Diagram of the nucleation of thin layers. a) The arrival of atoms on a substrate, b) The morphology of the substrate [10].

***b*) Coalescence** The nuclei grow in size but also in number until they reach a maximum nucleation density. This as well as the average size of these nucleus also called islets depend on a certain number of parameters such as the energy of the sprayed species, the rate of spraying, the energy of activation, adsorption, desorption, thermal diffusion, substrate temperature, topography and chemical nature of the substrates .

A nucleus can grow at the same time parallel to the substrate by a surface diffusion phenomenon of the pulverized species. It can also grow perpendicular to the substrate by adding sprayed species. In general the lateral growth in this stage is much more important than the perpendicular growth. figure 1.4 represents the phase of coalescence.

***c*) Growth** The last step in the film manufacturing process is the coalescing step in which the islets begin to cluster. This tendency to form larger islets is improved by the growth of the surface mobility of the adsorbed species. This improvement is obtained by increasing the temperature of the substrate. These larger islets still grow, leaving channels and holes on the substrate. The structure of the film in this step changes

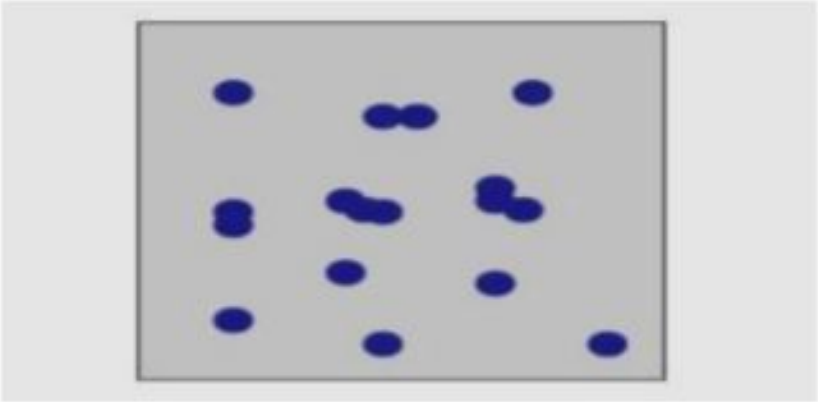

Figure 1.5: Diagram representing coalescence [10].

from a type of discontinuous islands to a type of porous networks .A continuous film is formed by filling the channels and the holes [10].

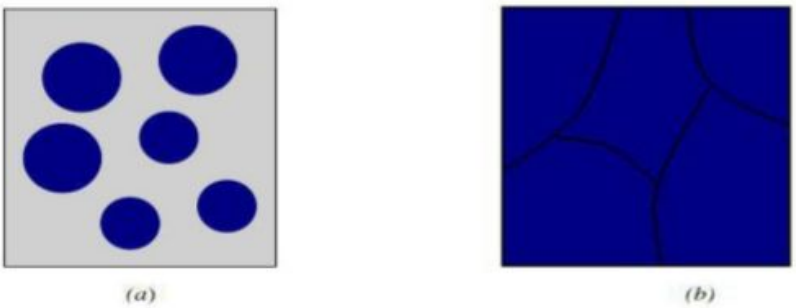

Figure 1.6: The growth of thin layers. a) Step after coalescence, b) Growth [10].

1.1.5 Applications of thin films

During 20th century, more sophisticated applications diversified in the following fields [[11]-[11]].

- **Microelectronics:**It was developed from the 1960s thanks to the use of increasingly thin conductive or insulating layers, and can be found under types of passivating layers (electronic contact), PN junction, transistor diode, piezoelectricity, laser, LED lamps, superconductors, etc.

- **Optics:**While retaining the aesthetic applications, the optical applications of the layers have made it possible to develop more effective radiation sensors, such as antireflective

layers in solar cells, anti-reflective treatment of camera lenses, photo detection, display of screens dishes, ophthalmic applications, optical guides (architecture energy checks, vehicles, energy conversion, etc.).

- **Mechanics:**Tribological coatings (dry lubrication, resistance to wear, erosion, abrasion, diffusion barriers) micro-systems... etc.
- **Chemistry:**The main applications of surface coatings are oriented towards better corrosion resistance by the creation of a waterproof film (corrosion resistance), gas sensor, catalytic coatings and protective layers.
- **Thermal:**The use of a thermal barrier layer (TBC) decreases for example the surface temperature of the metal of the fins of the reactors thus making it possible to improve the performances of the reactors (increase in the internal temperature).
- **Biology:**Biological micro sensors, biochips, biocompatible materials... etc.
- **Micro and Nanotechnologies:** Mechanical and chemical sensors, micro fluidics, actuators, detectors, adaptive optics, nano-photonics... etc.
- **Magnetic:** Information storage (computer memory), security devices, sensors.
- **Decoration:**Watches, glasses, jewelry, household equipment, etc [12].

1.2 Semiconductors

1.2.1 Definition of semiconductor

The semiconductor is a material in the solid or liquid state that conducts electricity at room temperature but less easily than a conductive metal. At low temperatures, pure semiconductors behave like insulators; at high temperatures or in the presence of light or impurities the conductivity of semiconductors increases sharply and can even become comparable to that of metals [13].

1.2.2 Band Gap

In solid materials, interactions between atoms "smear" the valence shell into a band of energy levels called the valence band. Valence electrons are confined to that band. When an electron acquires enough additional energy, it can leave the valence shell, become a free electron, and exist in what is known as the conduction band. The difference in energy between the valence band and the conduction band is called an energy gap or band gap. This is the amount of energy that a valence electron must have in order to jump from the valence band to the conduction band. Once in the conduction band, the electron is free to move throughout the material and is not tied to any given atom. Figure 1.7 shows energy diagrams for insulators, semiconductors, and conductors.

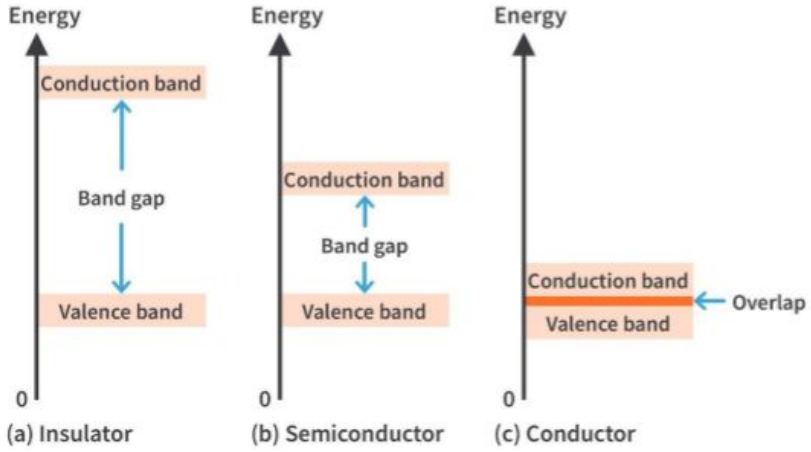

Figure 1.7: Energy diagrams for the three types of materials

1.2.3 Types of Semiconductors

Semiconductors can be classified as: Intrinsic Semiconductor and extrinsic Semiconductor. Extrinsic Semiconductors are further classified as: a n-type Semiconductors and p-type Semiconductors.

In **p-type semiconductors**, holes are the majority carriers and electrons are the minority carriers. In **N-type semiconductors** electrons are the majority carriers and the holes are the minority carriers.

1.2.4 PN Junction

When a n-type silicon comes into contact with a p-type silicon they form what is known as a junction (Figure 1.8). The current can only pass in one direction. In fact, if we look at it in terms of energy, the electrons from the “n” side do not have the same energy as those from the “p” side; these latter electrons take part in the bonding process and are strongly bonded in the crystalline lattice. The “n” electrons, which are free, are now more energetic. What happened to their contact? What happens when we try to join two liquid bodies of two different levels? What happens is that there is a flow of one into the other. But here, the liquid is electrically charged, and the passage of the electrons from the “n” crystal to the “p” crystal leads to the appearance of a difference in potential which balances the system. This is equal to the energy difference in volts of the banded-electron linked to the free electron states as is the case for silicon. If we directly polarize the atom, where the negative pole is on the “n”, then the current will flow. As a consequence, the “n” and “p” parts of a crystal automatically isolate themselves, which is a property used in semi-conductor components[14].

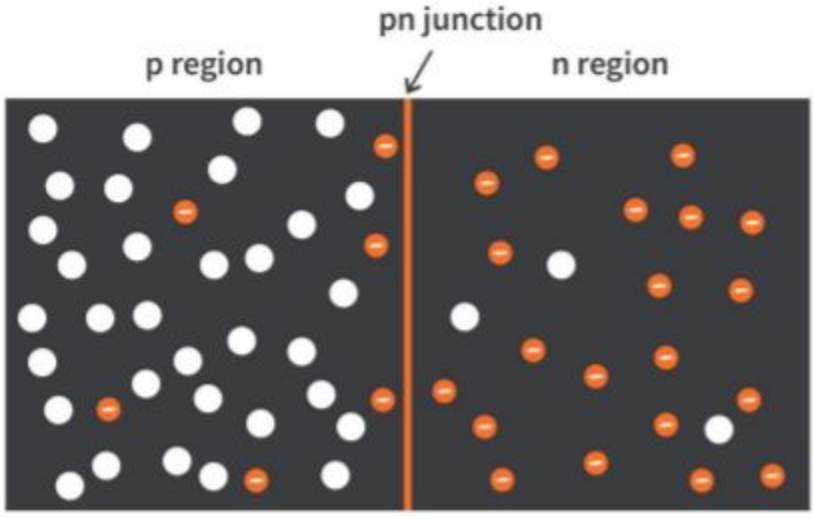

Figure 1.8: PN junction

1.3 Cupric (tenorite) oxide CuO

Copper (II) oxide is an inorganic compound with the formula CuO. A black solid, it is one of the two stable oxides of copper, as a mineral, it is known as tenorite. It is a product of copper mining and the precursor to many other copper-containing products and chemical compounds.

1.3.1 Reason for choosing copper oxide

This phase of copper oxide is used in various applications such as solar cells, gas sensors, and photocatalysis applications. Other reason supporting this choice is chemical stability, excellent electrical conductivity, non-toxicity, low cost yielding economical advantages, .industrializablility [[15], [16], [17]].

1.3.2 Crystallographic structure

CuO or tenorite oxide is distinguished from the transition metal monoxides 3d by its monoclinic structure. It is a black ionic solid having as fusion temperature $\mathbf{1134°}\boldsymbol{C}$. In this structure, copper is at the center of square planes defined by oxygen anions (Figure 1.9). Tenorite crystallizes in the $\boldsymbol{C2/c}$ space group with lattices parameters defined in Table 1.1.

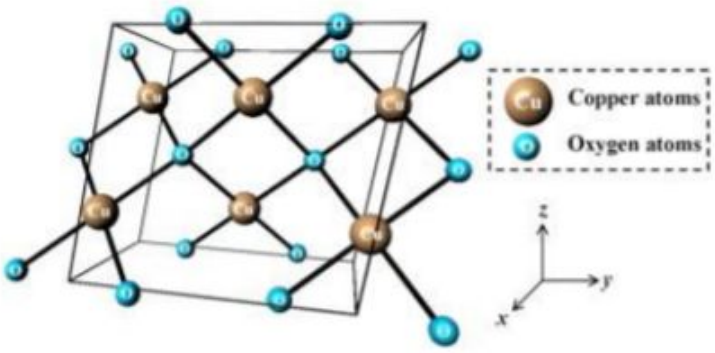

Figure 1.9: Schematic representation of the crystallographic structure of CuO: the brown spheres represent the $\boldsymbol{Cu^{2+}ions}$ and the bleu spheres the $\boldsymbol{O^{2-}ions}$.

Crystallographic properties of CuO	
Space group	C2/c
Unit cell	$\boldsymbol{a = 4.6837\mathring{A}}$ $\boldsymbol{b = 3.4226\mathring{A}}$ $\boldsymbol{c = 5.1288\mathring{A}}$ $\boldsymbol{\beta = 99.548^{\circ}}$ $\boldsymbol{\alpha, \gamma = 90^{\circ}}$
Cell volume	$\boldsymbol{81.08\mathring{A}^3}$
Cell content	4[CuO]
Distances Cu-O Cu-Cu O-O	 $\boldsymbol{1.96\mathring{A}}$ $\boldsymbol{2.62\mathring{A}}$ $\boldsymbol{2.90\mathring{A}}$
Rayons ioniques	$\boldsymbol{Cu^{2+} = 0.73\mathring{A}}$ $\boldsymbol{O^{2-} = 1.24\mathring{A}}$

Table 1.1: Crystallographic properties of CuO [18].

1.3.3 Structural properties

Deposition conditions and method are strongly affecting the thin film growth. Based on findings of previous studies, the main parameter must be controlled in order to achieve a high quality film is deposition temperature. The effect of deposition temperature, annealing temperature, and substrate temperature on present phase and (hkl) orientation of CuO thin films by several of deposition techniques is shown in Table 1.2. The experimental conditions must be carefully chosen in order to obtain the desired structural properties. For example: some authors agreed that the increase in the substrate temperature improves the films crystallinity and yields to the change from amorphous to polycrystalline structure.

1.3.4 Physical and chemical properties

Pure cupric oxide is black solid with a density of $\boldsymbol{6.32g/cm3}$ and insoluble in water. It melts above $\boldsymbol{1134^{\circ}C}$ with some loss of oxygen. Table (1.3) regroups some physical and chemical properties of cupric oxide.

Deposition method	Parameter	Present phase	(hkl) orientation
Thermal decomposition	Temperature 400°C 400°C	CuO CuO	(002)(111) (002)(111)
Thermal oxidation	Annealing Temperature 150°C 200°C 250°C 275°C-1000°C	Cu,$\boldsymbol{Cu^2O}$ $\boldsymbol{Cu^2O}$ $\boldsymbol{Cu^2O}$,CuO CuO	(111)(200) (111)(200) (111) (111)
Spray pyrolysis	Substrate temperature 250°C 350°C 450°C	$\boldsymbol{Cu^2O}$,CuO $\boldsymbol{Cu^2O}$,CuO,$\boldsymbol{Cu^2O}$,CuO $\boldsymbol{Cu^2O}$,CuO	(111)(200) (111)(200)(200)(020) (111)(200)
Spin coating	Annealing temperature 300°C-400°C 500°C-700°C	CuO CuO	(002) (111)(112) (110)(002)(111)(200) (112)(221)(004)(023)

Table 1.2: Structural properties of CuO thin film deposited by different method.

Cupric oxide CuO	
Chemical names	copper(II)oxide Cuprico xide Copper monoxide Copper oxide(CuO) Oxocopper
Molecular	CuO
Appearance	black to brown powder
Solubility in water	Insoluble
Molecular mass	79.55(g/mol)
Density	$\boldsymbol{6.32(g/cm^3)}$
melting point	$\boldsymbol{1134°C}$
Boiling point	$\boldsymbol{2000°C}$
Refractive index	1.4[21]
Hole effective mass	$\boldsymbol{0.2m^2}$[21]
Hole mobility	$\boldsymbol{0.1-10(cm^3/Vs)}$[21]
Magnetic suseptibility	$\boldsymbol{+238.9\times10^{-6}cm^3/mol}$
Refractive index($\boldsymbol{n_D}$)	2.63

Table 1.3: Physical properties of CuO[18].

1.3.5 Electrical properties

Copper oxide is a p-type semiconductor at room temperature. Its direct band gap Eg ranges from 1.2 to 2.1 eV. Because of the existence of acceptor levels attributable to copper vacancies, oxides with metal defects by cationic vacancies or oxides with excess oxygen by interstitial anions releasing holes generally endow to the CuO semiconductor material a low conductivity. There have been notable disparities seen in resistivity levels though with a pronounced correlation between resistivity and the elaboration process employed. The conductivity of CuO can be controlled in a low partial pressure environment during its formation. Additionally, CuO is sensitive to the presence of adsorbed molecules, indicating its significant potential for chemical and environmental detection. This sensitivity is even observed with a small quantity of impurities in the compound, highlighting its temperature stability [[22]-[23], [24], [25]].

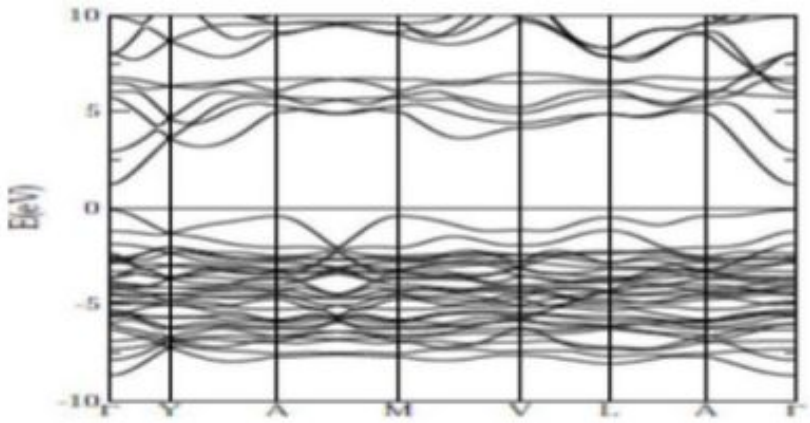

Figure 1.10: Band structure of CuO calculated using the DFT+U method [26]

1.3.6 Optical properties

Thin films of CuO have a transparency between 0 and **80%** in the visible region and a refractive index varies in the range of 1.5 to 3.5. Native point defects are intrinsic in semiconductors, they play an important role in the electronic properties of semiconductors. The formation energies of these defects are also calculated for three different types of native point defects: vacancies $(\boldsymbol{V_{Cu}, V_O})$, antisite $(\boldsymbol{Cu_o, O_{Cu}})$ and interstitial $(\boldsymbol{Cu_i, O_i})$ defects. The optical properties of CuO vary according to various factors such as: grain size, substrate temperature, thickness, doping concentration, strain strain, structural parameters, defects

and disorder, as well as deposit techniques and conditions [27].

Under the action of a high-energy light beam or electron bombardment, copper oxide emits photons. This phenomenon corresponds to luminescence. Depending on the conditions of elaboration, different luminescence bands were observed. The UV and visible luminescence are due to the near-band-edge (NBE) emission or inter band emission and to the different defect states

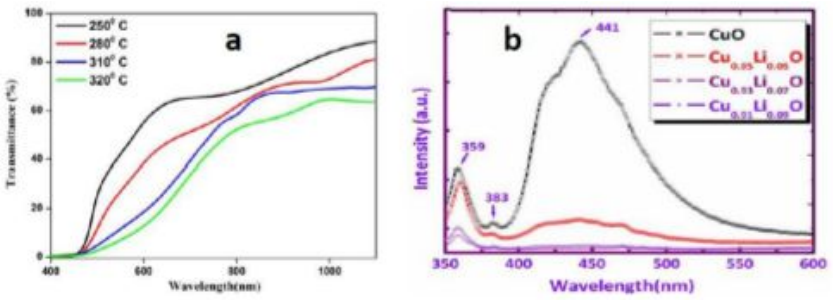

Figure 1.11: Transmittance (a) [28] and photoluminescence (b)[29]of CuO thin films

1.3.7 Applications of CuO thin films

CuO is a promising material for various applications due to the abundance of its components in nature, low-cost production, good thermal stability, and electrochemical properties. This combined property enables CuO thin films to be a serious candidate for several applications namely:solar cells [30], gas sensors [31] and photocatalysis.

Solar cells

Solar cell technology for future energy has improved in several technical areas. Cost reduction is one of the most crucial concerns in producing traditional solar cells which use silicon as a material semiconductor. [32]. Due to the high cost of silicon solar cells, new photovoltaic devices need to be developed using inexpensive, non-toxic materials and energy-efficient methods [33]. CuO semiconductors have the qualities of suitable materials with high optical absorption coefficients, low thermal emissivity and low manufacturing costs. CuO is an exciting material for solar cells because the material under consideration exhibits p-type semiconductor characteristics with its band gap closely approximating the ideal energy band gap for efficient utilization in solar cell applications [32]. Producing solar panels using cupric

oxide as a potential active layer has therefore attracted much attention. Various deposition processes have been used, including electro-deposition, RF sputtering, sol-gel, and plasma evaporation. The characteristics of solar cells based on CuO are intricately linked to the method of deposition. For example, the ZnO/CuO interface of solar cells produced by the electro-deposition process has a higher density of defects which significantly impacts the solar cells efficiency. The layers utilized in this context are ZnO, Cu2O, ZnO:Sn and C60, and they all impacts the solar cells efficiency. By manipulating the optical and chemical characteristics of the buffer layer, several current studies seek to increase the efficiency of solar cells. Furthermore, diligent endeavors have been undertaken to develop a thin film with soft and smooth consistency as a window layer for solar cells based on copper oxide (CuO) [34].

Gas sensor

For years, metal oxide semiconductors (MOS) have been utilized for the detection of reducing gases, including hydrogen, ethanol, carbon monoxide (CO) and hydrogen sulfide ($\boldsymbol{H_2S}$). Such materials like pure phase CuO or CuO bonded to other MOS in a composite material have been explored. The growing interest in various CuO nanostructures such as nanowires and thin films can be attributed to their very high surface-to-volume ratio. The enhancement of device performances in semiconductor nanostructures is thus anticipated [35]. The p-type copper oxide semiconductor under investigation for gas sensing applications has garnered significant attention in academic research due to its advantageous characteristics, including its affordability, exceptional stability, and non-toxic nature. For the detection of various gases, several researchers have focused on creating unique CuO nanostructures [36]. Gas sensors have gathered much interest as integrated devices into daily life for precise monitoring and control of ambient humidity for human comfort and prospective applications in industries such as robotics, aerospace, agriculture,and health [37].

Photocatalytic application

Multiple studies have shown that the use of CuO for the photocatalytic degradation of organic contaminants in aquatic environments is possible. The utilization of CuO has been employed in the process of photocatalysis degradation of methylene blue, facilitated by ex-

posure to sun irradiation [38]. To control the efficiency of photocatalysis, one can use an active medium for the preparation of the pollutants such as the use of lactic acid (LA), methanol (MeOH), triethanolamine (TEOA) and so on. The photocatalyst efficiency for of H2 generation in solution has been reported to improve with the increasing redox potential of the hole scavenger. Currently, the process of producing H2 from CuO based on photocatalysts is usually carried out in an aqueous solution of MeOH [39]. Research studies have revealed the superior stimulating activity of metallic nanoparticles using copper oxide as the perfect support [40]. Hence, CuO is a good catalyst in the rose bengal (RB) dye degradation. In particular, A. Al Gamdi and al. [41] studied a thin layers of CuO deposited by RF sputtering in 600 s. A degradation of **100%** of methylene blue under visible light in 3 hours was observed. In addition, another study on the Au-CuO2-CuO composite deposited by RF magnetron sputtering method showed dye degradation with percentages **73.1%** for methyl orange and **86.2%** for methylene blue in 28 mins of sun exposure, see Kavita Sahu and al. [42].

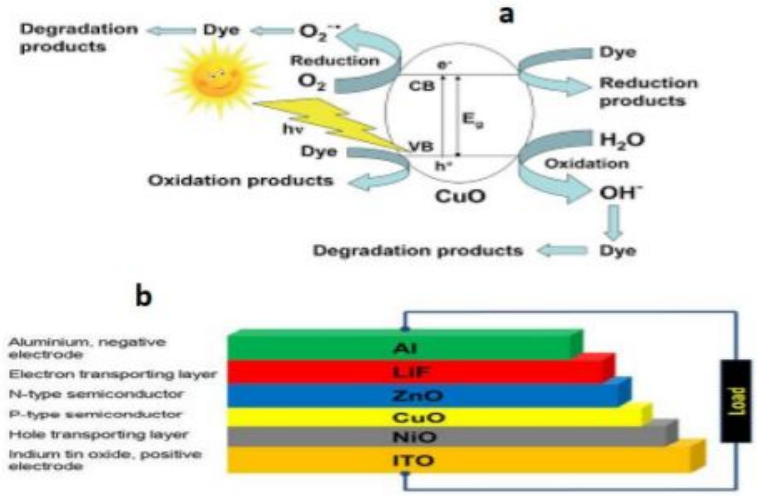

Figure 1.12: Some applications of CuO; photocatalysis [43], solar cell [44]

CHAPTER

2

METHODS OF DEPOSITION AND CHARACTERIZATION

This chapter contains the different methods of the deposition thin films include a description of the chosen deposition procedures and the techniques used to characterize thin films.

2.1 Thin films deposition methods

Generally, any thin film deposition follows the sequential steps: a source material is converted into the vapor form (atomic/molecular/ionic species) from the condensed phase (solid or liquid), which transported to the substrate and then it is allowed to condense on the substrate surface to form the solid film [45]. Depending on how the atoms/molecules/ions or clusters of species are created for the condensation process, the deposition techniques are broadly classified into two categories (Figure 2.1): physical methods and chemical methods.

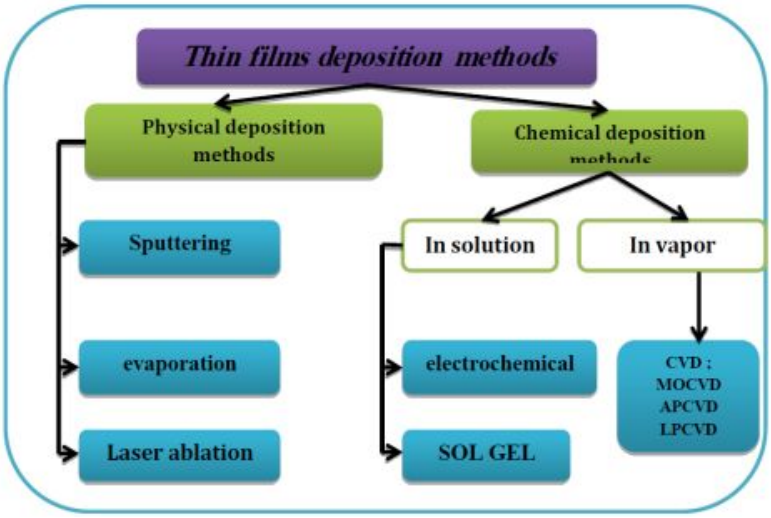

Figure 2.1: Classification of thin film deposition techniques [46].

2.2 Criteria for selection of deposition methods

The selection of a specific technology for the deposition of thin films can be based on a variety of considerations. A multitude of thin films of different materials can be deposited for a large variety of applications; hence, no general guidelines can be given of what the most suitable deposition technology should be. In selecting an appropriate deposition technology for a specific application, several criteria have to be considered. In order to optimize the desired film characteristics, a good comprehension of the advantages and restrictions applicable to each technique is necessary. The choice of a specific deposition technique related to some factors, they are:

- The material to be deposited.
- The rate of deposition.
- Limitations imposed by the substrate, e.g.: maximum deposition temperature.
- Adhesion of the deposits to a substrate.
- Throwing power.
- The purity of target material.
- Availability of the required equipment.

- Cost.
- Ecological considerations.
- The abundance of the material (to be deposited).

2.3 Different deposition techniques

The properties and versatility of the thin films can be obtained by selecting proper technique of film deposition. Thin film deposition methods can be broadly classified as either chemical or physical methods. The difference between the chemical and physical thin film deposition methods depends upon the method of depositing thin film material on the substrate. In chemical deposition technique, fluid precursor is used which chemically react with the substrate. Since the thin film material is conducted through the fluid precursor, physical deposition is conformal approaching the substrate without preference to a particular direction. A conformal is an uneven interface with the body and has a constant thickness on horizontal and vertical surfaces [47].

2.3.1 Physical vapor deposition (PVD)

Physical Vapor Deposition (PVD) mainly includes evaporation, spraying in all its forms and laser ablation. The most widely used PVD methods are molecular beam epitaxy, cathodic sputtering.

1. **Sputtering:** Sputtering is a technique used to deposit different materials such as metals, refractory materials, dielectrics, and ceramics. The principle of this technique is the bombardment of the material to be deposited (target) by neutral gas ions generally argon, under the effect of bombardment atoms torn from the target and deposits on the substrate located in front of the target. If the atmosphere (gas) of the discharge is chemically neutral, the sputtering is called simple. However, if it consists of active gases such as oxygen $\boldsymbol{O_2}$ or nitrogen $\boldsymbol{N_2}$, sputtering is said to be reactive. The basic scheme of operation of the sputtering is shown in figure 2.2.

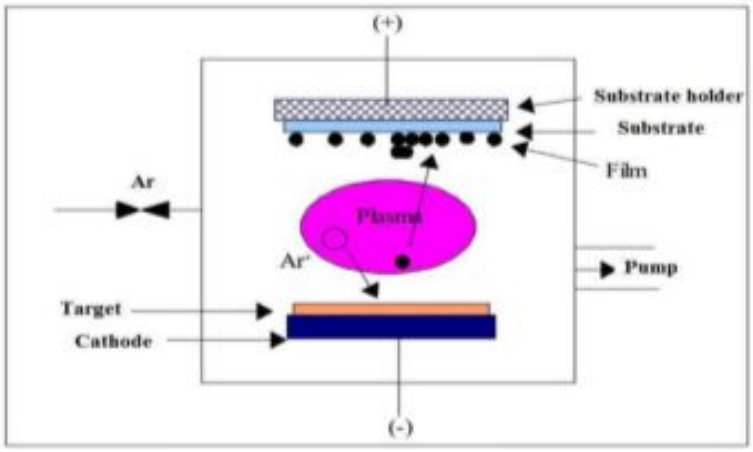

Figure 2.2: The operating principle of sputtering [48].

There are two types of cathodic sputtering depending on the mode of creation of the plasma or the nature of the target (conductive or insulating): direct cathodic sputtering (DC) only in the case of the sputtering of conductive materials and sputtering radiofrequency (RF) which allows the spraying of conductive materials or insulating materials. There are many parameters that affect the deposition process such as base vacuum, sputter gas pressure during deposition, sputter power, target and substrate temperature, etc... The magnetron device has been used to limit the disadvantages and increase the efficiency of the sputtering.

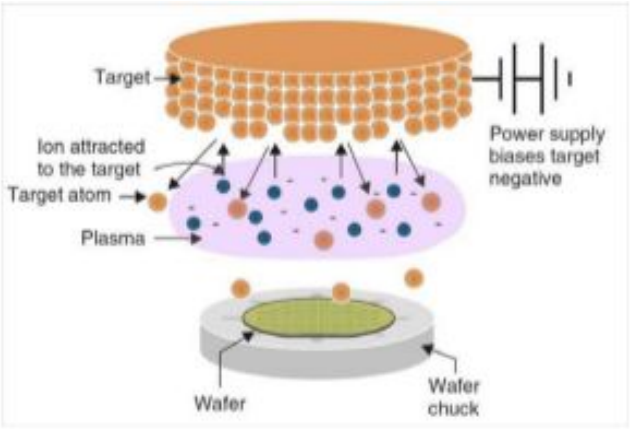

Figure 2.3: Cathodic sputtering: accelerated $\boldsymbol{Ar}^{+}$ ions extract atoms from the target [49].

2. **Molecular Beam Epitaxy (MBE):**

Epitaxy is a compound of two Greek words Epi = on, Taxi = arrangement. It is defined as the formation of a monocrystalline layer called (the epitaxial layer) on a monocrystalline substrate [50]. Molecular beam epitaxy is a method for developing thin films at low temperature with excellent crystalline quality and very low roughness in a very high vacuum ($< \mathbf{10^{-10}}$ Torr). The principle of this technique, Figure 2.4, is based on the reaction of atomic or molecular fluxes on a monocrystalline substrate which brought to an adequate temperature [50].

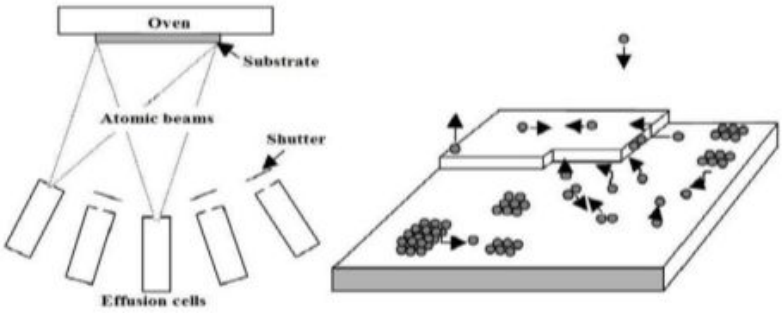

Figure 2.4: The operating principle of MBE [50].

As shown in figure 2.4, the growth process of the molecular beam epitaxy can be summarized in the following steps [50]:

1) Deposition of atoms onto the surface of the substrate

2) Nucleation process (creation of di-atomic islands)

3) Growth of islands by coalescence

4) Formation of a layer by coalescence of islands

Molecular beam epitaxy has the following advantages [50]:

- The low growth rate that allows doping at the atomic level
- Possible controls and in situ analysis (RHEED; Auger XPS)
- Very precise control of the thicknesses of the thin layers
- The ability to control all the steps automatically

- No boundary layer.

3. **Pulsed Laser Deposition:**

   Pulsed Laser Deposition (PLD) is a deposition technique that has the advantage of transferring the stoichiometry of the target to the prepared layer, in this method a laser beam focused on a depositing material (target) placed in an ultrahigh vacuum chamber. Under the effect of this laser beam, an amount of the material is pulled away from the target in the form of a dense and light vapor (plasma) and deposited on the substrate placed opposite as presented in Figure 2.5.

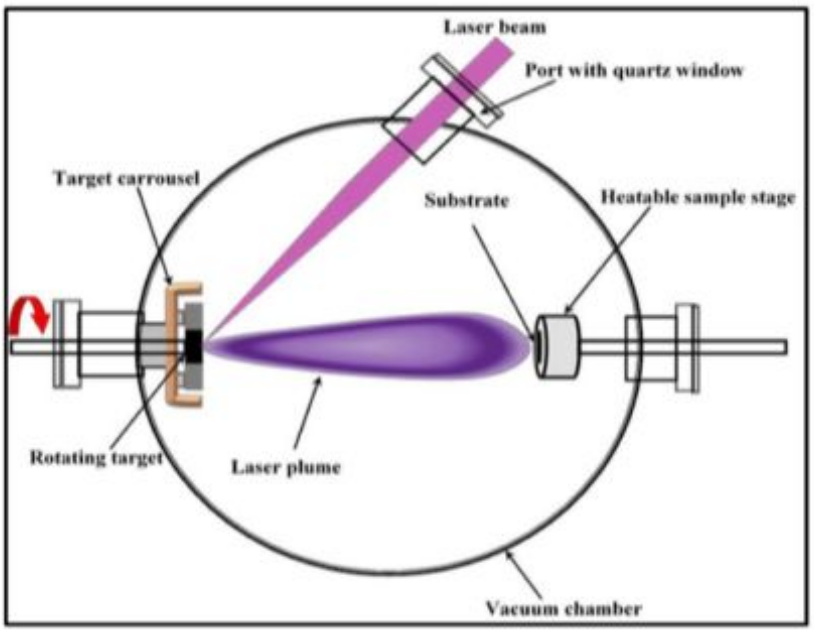

Figure 2.5: Schematic diagram of the Pulsed Laser Deposition (PLD) technique [51].

Laser ablation has a number of advantages, it enables the deposition at room temperature and the coating of all types of the substrate [51], and it also allows the manufacture of the complex composition of materials in thin layers.

4. **Thermal evaporation:**

   The thermal evaporation process contains evaporating source materials in a vacuum chamber below $\mathbf{10^{-6}}$ Torr and condensing the evaporated particles on a substrate. In this process, thermal energy is provided to a source from which atoms are evaporated for deposition in the substrate. Heating of the source material can be finished by any

of which the material to be evaporated is attached. Larger volumes of source material can be heated in crucibles of refractory metals, Oxides or Carbon by resistance heating, high-frequency induction heating, or electron beam evaporation. The evaporated atoms travel through reduced background pressure in the evaporation chamber and condense on the growth surface. The deposition rate or flux is a function of the travel distance from the source to the substrate, the angle of impingement onto the substrate surface, the substrate temperature Ts, and the base pressure. The conventional thermal evaporation system is mentioned in Figure 2 .6 [[47]-[52]].

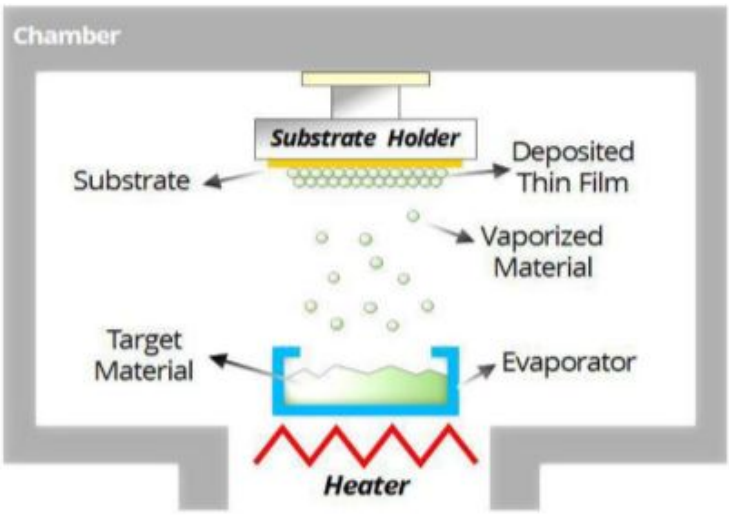

Figure 2.6: Schematic diagram of thermal evaporation system [53].

2.3.2 Chemical deposition

1. **Chemical Vapor Deposition (CVD):**
   The CVD technique consists of developing materials in the form of thin layers from gaseous precursors that chemically react to form these layers on a heated substrate [54], as shown in Figure 2.7. The CVD process can be summarized in five steps [50]:

   - Transporting reactive gas species (or species) to the substrate.
   - Adsorption of the reactants on the surface.
   - Surface reaction and film growth.
   - Desorption of volatile secondary products.

- Transport and evacuation of gaseous products to the reactor outlet.

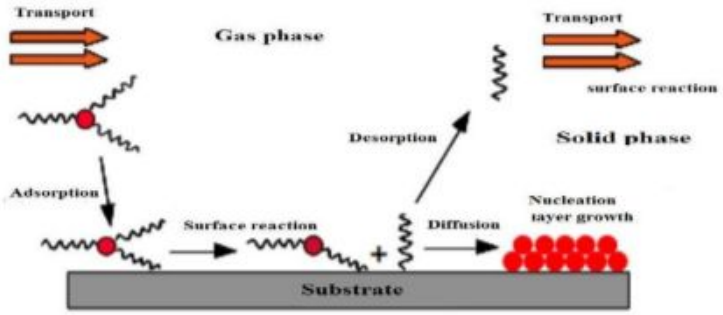

Figure 2.7: Schematic diagram of thermal evaporation system [50].

The improvement of this technique is to reduce the deposition temperature and the reactor pressure and remedy the low volatility of the precursors. Several CVD type techniques can be given [55]:

- APCVD: (Atmospheric Pressure Chemical Vapor Deposition) deposition under atmospheric pressure.
- LPCVD: (Low-Pressure Chemical Vapor Deposition) low-pressure deposition.
- MOCVD: (Metal Organic CVD) the use of organometallic precursors.
- PACVD: (Plasma Assisted Chemical Vapor Deposition) with the assistance of a plasma.

2. **Sol-Gel:**

- **Sol:**a stable suspension of colloidal solid particles or polymers in a liquid.
- **Gel:**porous, three-dimensional, continuous solid network surrounding a continuous liquid phase.

Sol-gel is a chemical synthesis technique for preparing glasses, gels and ceramic powders. For the purposes of many theses, it will serve as an easy way to make high purity glass in solution form at room temperature. In the sol-gel process, a system of colloidal particles in a solution (sol) becomes a macroscopic material (gel), which is interpenetrated by a liquid [56].

There are different sol-gel methods:

Dip Coating:In a dip-coating process, a substrate is dipped into a liquid coating solution and then is dragging from the solution with controlling withdrawal speed as described in figure2.8. Generally, the thickness increases at faster dragging speed. The measurement of thickness by the equilibrium of forces at the stagnation point on the liquid surface [57]. The thickness is primarily affected by fluid viscosity fluid density, and surface tension. Therefore, a faster dragging speed pulls more fluid up onto the substrate before it has time to flow back down into the systemin, should be occur. While excellent for producing high- quality, uniform coatings, requires precise control and a clean environment. The applied coating may remain wet for several minutes until the solvent evaporates. This process can be accelerated by heated drying. Dip-coating technique is almost used to fabricate transparent layers of oxides on a transparent substrate with a high degree of planarity and surface quality [58].

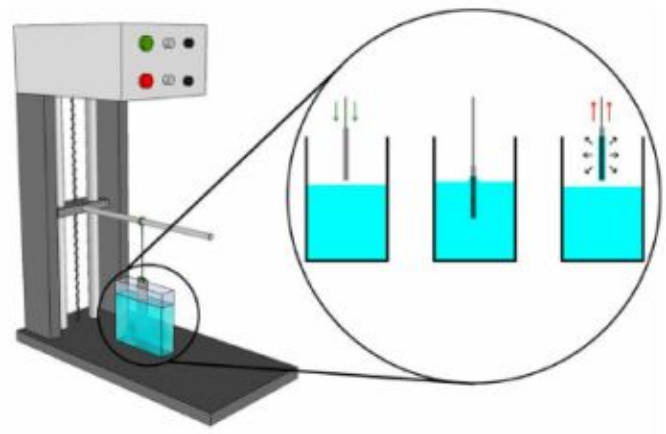

Figure 2.8: Schematic model describing the film formation during the dip-coating process [58].

Spin Coating: The precursor is dropped onto the centre of a spinning substrate which then spreads out quickly and evaporates the solvent, see figure 1.16. The Spin coating an exemplary process includes depositing a small puddle of a solution onto the center of a substrate and then spinning the substrate at high speed (typically around 3000 rpm) [59]. Centripetal acceleration will cause most of the resin to spread to, and eventually off, the edge of the substrate, leaving a thin film of material on the surface. Final film thickness and other properties will depend on the nature of the fluid material

(viscosity, drying rate, percent solids, surface tension, etc.) and the parameters chosen for the spin process. Factors such as final rotation speed, acceleration, and fume exhaust affect the properties of the coated films. One of the most important factors in spin coating is repeatability, as subtle variations in the parameters that define a spin-coating process can result in drastic variations in the coated film [58].

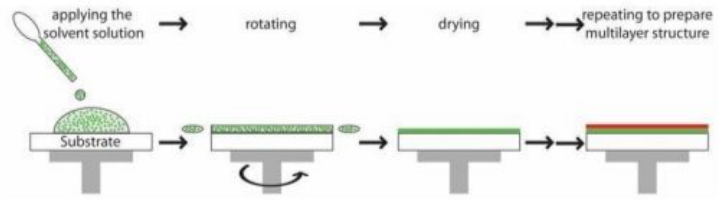

Figure 2.9: Schematic model describing the film formation during the spin-coating process [58].

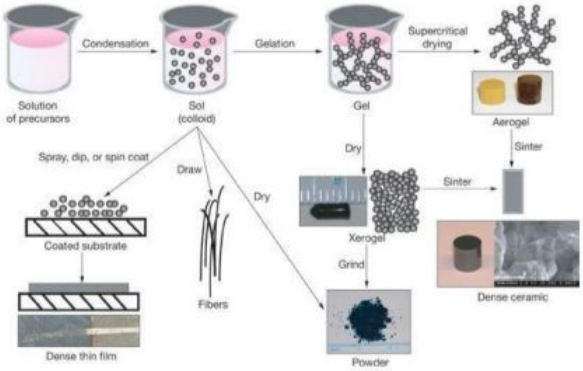

Figure 2.10: Synthesis of various forms of materials by the sol-gel method [60].

3. **Chemical bath deposition:**

   The chemical bath deposition (CBD) is also recognized as controlled precipitation; it has been applied since to deposit films of many different semiconductors. It is currently attracting great attention as it does not necessitate sophisticated instrumentation like vacuum system and other expensive equipment. All that is required is a vessel to include the solution (an aqueous solution made up of a few usually common, chemicals) and a substrate on which deposition is required. It offers a bottom-up approach to prepare nano-crystalline materials in thin film form with better particle size controlled,

particle shape, size distribution, particle composition, the degree of particle agglomeration, the conventional thermal evaporation system is presented in figure 2.9 [61].

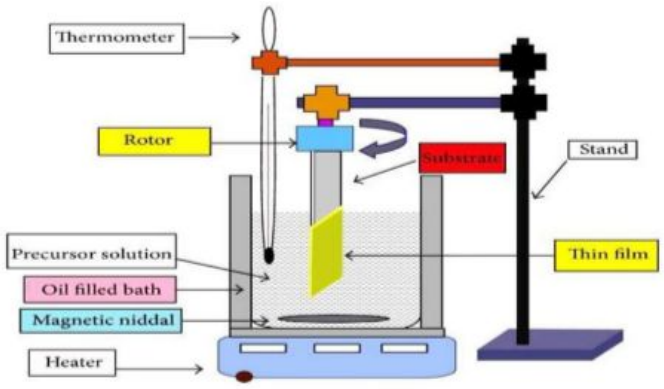

Figure 2.11: Schematic diagram of chemical bath deposition system [61].

4. **Chemical Spray Pyrolysis Technique:**

The thin layers used in this study were prepared by spray pyrolysis. This technique, which is an intermediary between pneumatic spraying and chemical vapor deposition, seems to be very simple and relatively cost-effective, particularly in terms of equipment cost .

a-Definition:

Spray pyrolysis is the most common name given to this technique. It consists of: spray and pyrolysis. Spray is an English word that indicates the jet of a liquid into fine droplets, propelled by a sprayer. Regarding pyrolysis, it is noted that it has various definitions: "pyrolysis is a process by which a solid (or liquid) undergoes, under the influence of heat and without interaction with oxygen or any other oxidants, degradation of chemicals into smaller volatile molecules" . This definition is similar to the thermal decomposition of a source to release a metal or a compound.

The Spray pyrolysis technique is a chemical deposition process being used in research to prepare thin and thick layers. Unlike in many other coating techniques, the spray technique represents a very simple and relatively cost-effective processing method (particularly in terms of relates to equipment costs). It offers an extremely easy technique for preparing films of any composition [62]. This technique consists in projecting a so-

lution containing the elements that we want to deposit on a heated substrate, all under a controlled atmosphere. For the synthesis of oxide films. The advantage of such a method is its simplicity and low material cost as well as good control of the deposition conditions (temperature of the substrate, concentration of the starting solution, etc.) [63].

There are Two methods are generally used to spray the solution containing the source material:

- **Pneumatic spraying:** The production of the fog is carried out by a compressed gas which sucks and bursts the liquid (Figure 2.12.a) [[64],[65]].
- **Ultrasonic spray pyrolysis:** The aerosol is generated from the high frequency vibrations produced within the solution, and localized towards the free surface of the liquid (Figure 2.12.b).

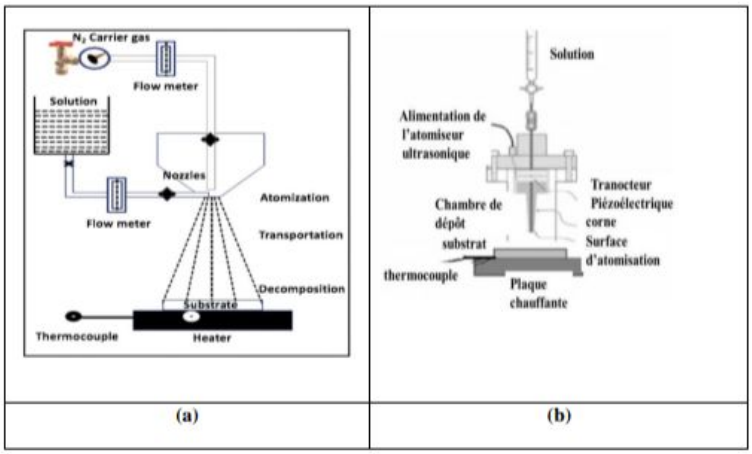

Figure 2.12: Spray pyrolysis method using; (a): Pneumatic, (b): Ultrasonic.

b-General principle of the spray process:

A solution of various reactive compounds is vaporized using an atomizer and then sprayed onto a heated substrate (Figure 2.13). The temperature of the substrate enables the activation of the chemical reaction between the compounds. The experiment can be conducted in air. This method, based on heat and mass transfer under unstable conditions, results in the movement of droplets towards the substrate .

The description of film formation by the spray pyrolysis method can be summarized as follows:

- Formation of droplets at the nozzle outlet and evaluation of their average size.
- Decomposition of the precursor solution on the substrate surface. Depending on the temperature of the substrate, several modes of decomposition of the source solution are possible. A classical CVD deposition occurs when the substrate temperature allows solvent evaporation and precursor vapor diffusion to the substrate, leading to a heterogeneous phase reaction upon contact.

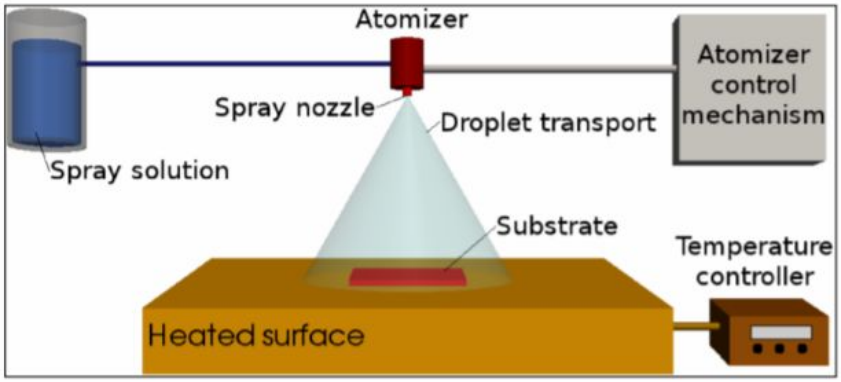

Figure 2.13: General schematic of a spray pyrolysis deposition process .

Despite its simplicity, spray pyrolysis has several advantages:

1. It offers an easy way to dope films with virtually any element in any proportion by simply adding a certain form of the spray solution.
2. Unlike closed vapor deposition methods, spray pyrolysis does not require high-quality targets, which is a major advantage for industrial applications.
3. The deposition rate and film thickness can be easily controlled across a wide range by changing the spray parameters, thereby eliminating the main drawbacks of chemical methods like sol-gel, which produce films of limited thickness.
4. Operating at moderate temperatures (100500C), spray pyrolysis can produce films with less robust materials.
5. By modifying the spray solution composition during the spraying process, it can be used to create layered films with composition gradients throughout the thickness.

Thermal decomposition of a source to release a metal or compound occurs. The substrate temperature provides the necessary energy, known as activation energy, to trigger the chemical reaction between the compounds. The experiment can be conducted in air and can be prepared in a chamber (or reaction chamber) under approximately 50 Torr vacuum.

Indeed, depositing thin layers by spray pyrolysis involves spraying a solution onto a heated substrate. The impact of the droplets on the substrate leads to the formation of a disc-shaped structure that undergoes thermal decomposition.

Factors influencing the properties of thin layers by the deposition process:

- Substrate temperature.
- Precursor solution: the solvent, type of salt, solution concentration, and additives influence the physical and chemical properties of the precursor solution.

There are numerous processes that occur sequentially or simultaneously during film formation by spray pyrolysis. These include atomization of the precursor solution, droplet transport and evaporation, diffusion on the substrate, drying, and decomposition of the precursor salt.

The microstructure of thin layers plays an important role in the optoelectronic properties of transparent semiconductor oxides.

2.4 Experimental Techniques for thin films characterization

We characterized our thin films by different techniques.

2.4.1 Structural characterization

X-Ray Diffraction (XRD) Principe

The crystalline structure of the thin films was analyzed by X-ray diffraction (XRD). This method, mainly applicable to crystallized materials (in powders, monocrystalline or polycrystalline), aims to specify the structure of materials, to measure lattices parameters, the

crystallites size, and the orientation statistic of crystallites. It must also make it possible to examine the state of constraint. A polycrystalline material is composed of a multitude of grains (crystallized domains considered as single crystals), themselves consisting of stacks of crystalline planes. These planes are defined by their Miller indices (hkl), characterizing the orientation of the lattice with respect to the elementary crystal lattice, and by their interticular distance dhkl. This distance can be measured by X-ray diffraction using Bragg's law.

$$\mathbf{2}\boldsymbol{d_{hkl}}\,\mathbf{sin}\,\boldsymbol{\theta} = \boldsymbol{n\lambda} \tag{2.1}$$

$\boldsymbol{d_{hkl}}$**:**Interreticular distance, that is, the distance separating two consecutive index planes (hkl). : Incidence angle of X-rays on the surface of the studied material. Also called a half deflection angle in geometry called $\boldsymbol{\theta - 2\theta}$ or symmetrical diffraction.

n:Order of reflection.

$\boldsymbol{\lambda}$**:**Wavelength of the X-ray beam of the same order of magnitude as the Interreticular distance.

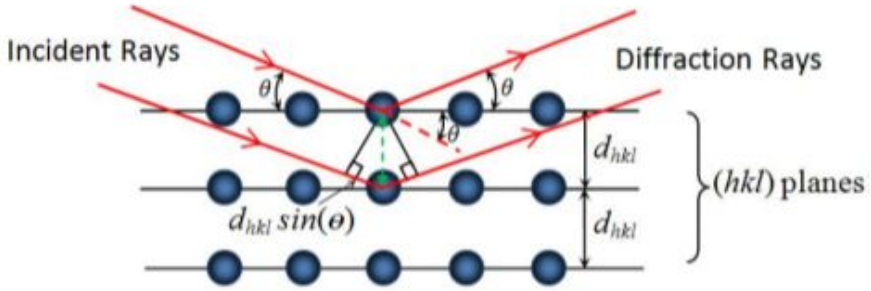

Figure 2.14: Principle of X-ray diffraction

Information obtained from the X-ray Diffractogram

Information obtained from the X-ray Diffractogram.

A. grain size:

From the X-ray diffraction pattern, the width generated in a peak which known as full width at half maximum (FWHM) (figure 2.15), can be used to calculate the mean crystallites sizes of the film in a direction perpendicular to the respective (hkl) planes,

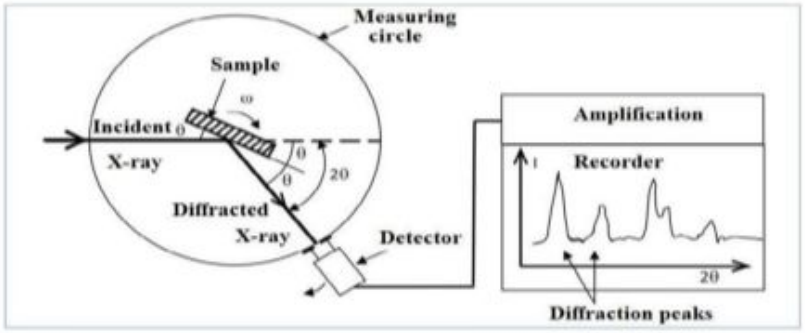

Figure 2.15: Schematic diagram of an X-ray diffractometer [67].

by using the Scherer's formula [[68], [69]], which is given as:

$$\boldsymbol{D_{hkl} = 0.9\lambda/\beta_{hkl}\cos\theta_{hkl}} \tag{2.2}$$

Where ($\boldsymbol{D_{hkl}}$) is the average grain size obtaining from the peak (hkl), ($\boldsymbol{\lambda}$) is the wave length of the X-ray beam, ($\boldsymbol{\beta_{hkl}}$) is the full width at half maximum intensity of the peak (hkl) and ($\boldsymbol{\theta_{hkl}}$) is the angel between the incident ray and the (hkl) scattering planes.

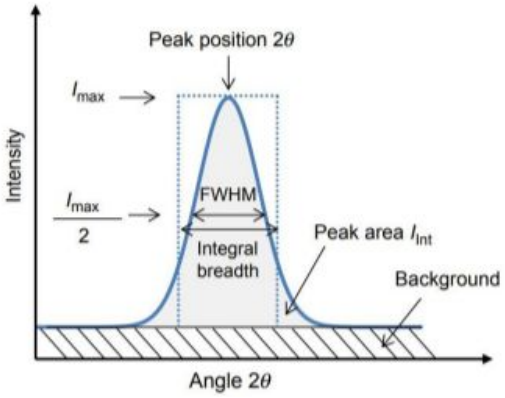

Figure 2.16: Full width at half maximum (FWHM) of an arbitrary peak [69].

B. Lattice parameters:

Experimentally, the Bragg law can be utilized by using X-rays of known wavelength($\boldsymbol{\lambda_0}$) and measuring ($\boldsymbol{\theta^{exp}_{hkl}}$), we can determine the inter planar spacing ($\boldsymbol{d^{exp}_{hkl}}$) of various planes in a crystal.

$$\boldsymbol{d^{exp}_{hkl} = \lambda_0/2\sin\theta^{exp}_{hkl}}$$

In our case, it is the monoclinic lattice of CuO whose expression of the distance between planes (hkl) is given in the following form :

$$\frac{1}{d_{hkl}} = \frac{1}{\sin\beta}\left(\frac{h^2}{a^2} + \frac{k^2\sin\beta^2}{b^2} + \frac{l^2}{c^2} - \frac{2hl\sin\beta}{ac}\right)^{\frac{1}{2}} \tag{2.3}$$

Lattice Constant (a_0) can be calculated of a particular cubic system through the following relation. (hkl) parameters and the inter planar spacing (d_{hkl}^{exp}) [70].

$$d_{hkl}^{exp} = \frac{a_{hkl}^{exp}}{\sqrt{h^2+k^2+l^2}}$$

The lattice parameters are substrate dependent. This gives rise to a mismatch between the substrate and the deposited thin films. The latter is responsible of the resulting strains and stresses.

The strain (ε) values of the films were estimated from the observed shift, in the diffraction peak between their positions in the XRD spectra via the formula [[71], [72]]:

$$\varepsilon = (a_{hkl}^{exp} - a_{hkl}^{rhe})/a_{hkl}^{rhe}$$

Where (ε) is the mean strain in thin films, **exp** hkl a is the lattice constant of thin films and the hkl a the lattice constant of bulk.

We can be also estimating the lattices micro strain (μ_ε) using another relationship [[73], [74]]:

$$\mu_\varepsilon = \beta\cos(\theta)/4$$

A dislocation is an imperfection within the crystal associated with the miss registry of the lattice in one part of the crystal with that in another part. Unlike vacancies and interstitial atoms, dislocations are not equilibrium imperfections, i.e. thermodynamic considerations are insufficient to account for involving dislocation as a matter of importance [75]. The dislocation density (δ) is the dislocation lines per unit area of the crystal can be evaluated from the grain size (D) using the formula [[74], [76]]:

$$\delta = 1/D^2(Lines/m^2)$$

C. Texture:

To describe the preferential orientation, the texture coefficient, TC (hkl) is calculated.

$$\boldsymbol{TC(hkl) = \frac{I(hkl)/I_0(hkl)}{\frac{1}{N}\sum_N I(hkl)/I_0(hkl)}}$$

Where $\boldsymbol{I(hkl)}$ is the measured intensity of a plane (hkl), $\boldsymbol{I_0(hkl)}$ is the standard intensity of the plane (hkl) taken from the JCPDS data and N is the number of diffraction peaks. The value $\boldsymbol{TC(hkl) = 1}$ represents films with randomly oriented crystallites, while higher values indicate the abundance of grains oriented in a given (hkl) direction [77].

Values $\boldsymbol{0 < TC(hkl) < 1}$ indicate the lack of grains oriented in that direction. As TC(hkl) increases, the preferential growth of the crystallites in the direction perpendicular to the hkl plane is the greater [77].

D. Dislocation density and number of grains:

The dislocation density ($\boldsymbol{\delta}$) can be calculated as the following [77]:

$$\boldsymbol{\delta = 1/D_{av}^2}$$

and number of crystallites can be calculated from the relation [77]:

$$\boldsymbol{N_0 = t/D_{av}^3}$$

Where t: is the thickness and $\boldsymbol{N_0}$: is the number of crystallites.

Raman spectroscopy

Definition:

Raman spectroscopy is an analysis the proposed an approach founded on the investigation of molecular vibrations. It complements infrared spectroscopy. It is based on the phenomenon of inelastic light scattering. The sample is excited by a monochromatic radiation, usually a laser beam [91]. The energy variation observed for the photon then provides information on the rotational and vibrational energy levels of the molecule or material concerned. Raman

spectroscopy provides a wide range of information. It can be used to characterize short-, medium- and long-range structural order, as well as a compound bond type and crystal structure. Its performance is particularly remarkable. It is the spectroscopic method with the best resolution (one micron) for identifying and characterizing compounds or phases. Its ability to identify amorphous systems is also unrivaled [[92],[93]].

Principle:

The principle of Raman spectroscopy is relatively simple. It involves shining monochromatic light onto the sample to be studied, and analyzing the scattered light. The scattering of monochromatic radiation by molecules gives rise to low-intensity radiation with frequencies different from those of incident radiation. These frequency changes, linked to the vibrational and rotational energies of the molecules, are specific to each molecule and the intensity of the scattered radiation is therefore characteristic of the material [94]. Scattering can be:

- ✓ Rayleigh or elastic : the incident radiation is elastically scattered without any change in energy.
- ✓ Inelastic scattering or Raman scattering (Stokes or Anti-Stokes).
- ✓ The diagram depicted below provides a visual representation of the Rayleigh and Raman scattering processes.
- ✓ If the frequency $\boldsymbol{v_{dif}(v_0 - v_{vib})}$ of the scattered photon is lower than that of the incident photon $\boldsymbol{v_0}$, the molecule gains vibrational energy (and the photon loses energy), forming a Stokes line.
- ✓ If, on the other hand, the incident photon is scattered at a frequency $\boldsymbol{v_{dif}(v_0 + v_{vib})}$ there is a loss of vibrational energy for the molecule (and a gain of energy for the photon), which corresponds to the anti-Stokes line of much lower intensity [[95],[93]].

2.4.2 Optical characterizations

Optical methods allow to characterize a large number of parameters. They have the advantage over electrical methods of being non-destructive and do not require the reaction, of ohmic contacts.

We distinguish two types of optical methods:

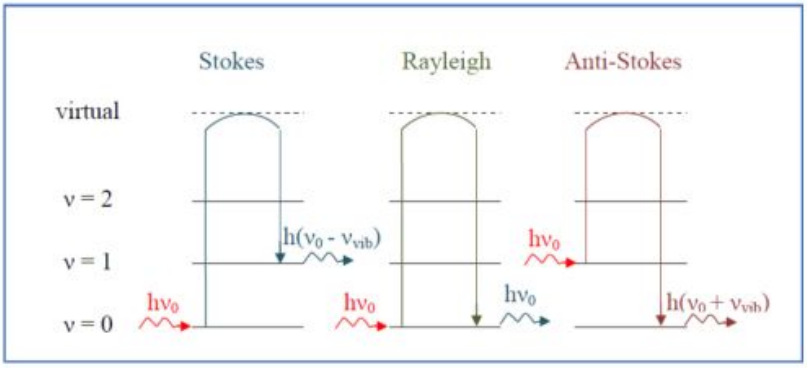

Figure 2.17: Raman and Rayleigh diffusion mechanisms in case of $\boldsymbol{v_0} >> \boldsymbol{v_{vib}}$.[93].

- The methods that study the optical response of the material to an excitation such as photo and cathodo-luminescence.
- Methods that analyze the optical properties of the material such as; transmittance and reflectance measurements and ellipsometry measurements. These spectroscopic measurements can determine the optical refractive index, the thickness of the material and the optical gap.

UV-Visible spectrophotometer

Ultraviolet-visible spectroscopy (UV-Vis) is used to measure the absorption spectrum of light by the sample in the ultraviolet and visible (UV / Vis) range, where the energy absorbed causes disturbances in the electronic structure of atoms, ions or molecules. One or more electrons absorb this energy to jump from a low energy level to a higher energy level.
This technique tells us about some optical properties of the material such as the estimation of the optical absorption threshold, the absorption coefficient, the optical gap and the refractive index. The optical transmittance spectra of the films involved in our work were carried out at room temperature by a UV-Visible UV-Visible UV 3101 PC spectrometer type Shimadzu, whose spectral range extends over a range of 350 nm to 800 nm. The UV-visible spectrophotometer consists of three main parts: the radiation source, the sample holder and the reference, and the measurement system. When a substance absorbs light in the in the ultraviolet and visible domains, the energy absorbed causes disturbances in the electronic structure of atoms, ions or molecules. One or more electrons absorb this energy to jump

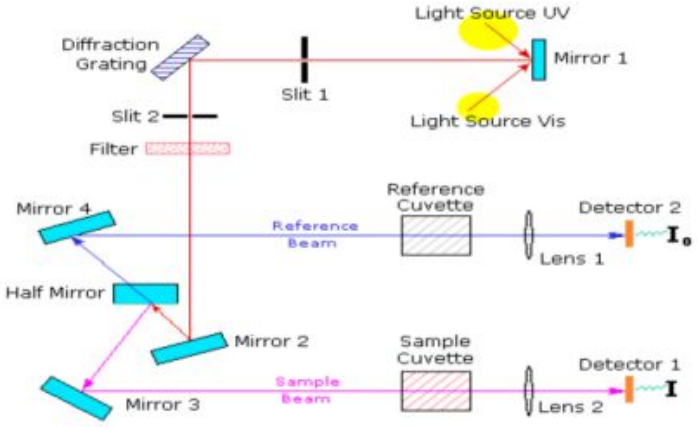

Figure 2.18: Schematic representation of the UV-Visible spectrophotometer[78]

from a low energy level to a high energy level. These electron transitions are in the visible range, from 350 to 800 nm and ultraviolet between 200 and 350 nm. A homogeneous medium traversed by the light absorbs a part of it, the different radiations constituting the incident beam are differently absorbed according to their energies, the transmitted radiations are then characteristic of the medium [[79], [80]].

The absorption of energy of photon equal or more than the band gap of the semiconductor induces a photo-excitation, while transmittance can be defined as the fraction of light of a given wavelength incident to a material that passes through that material.

Figure 2.17 presents the transmission curve of an arbitrary transparent thin film semiconductor. Incident photons with energies $\boldsymbol{hv \geq Eg}$ are absorbed, this absorption determined by the properties of the film (e.g. thickness and impurities), since there are numerous valence band electrons and the conduction band contains many empty states into which these electrons can be excited. A photon with energy $\boldsymbol{hv < Eg}$ is unable to excite a valence band electron to the conduction band, and as consequence they are transmitted, this explains why some semiconductors are transparent in certain wavelength ranges. Thus, for pure (intrinsic) semiconductors. There is negligible absorption of photons with $\boldsymbol{hv < Eg}$, a photon will be absorbed only if there are available energy states in the forbidden band gap due to chemical impurities or physical defects, this process is called extrinsic transition [81].

Information obtained from the UV-Visible transmittance spectra:

Much information is obtained about the properties of materials when they interact with electromagnetic radiation. When the light beam (photons) is an accident on an object, there

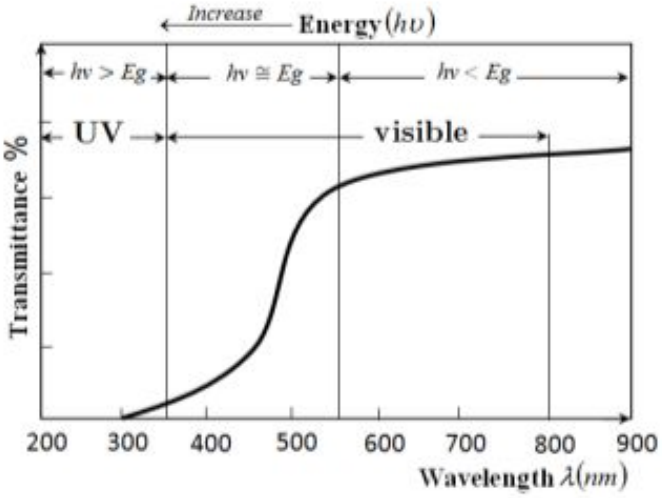

Figure 2.19: Presents the transmittance curve of a thin film of metal oxide semiconductor[81].

is some expected absorption, determined by the properties of the material.
In the following we will integrate the properties of films that can be deduced from the transmittance spectrum.

A. **Absorption coefficient:**

Absorption coefficient expresses the decrease in the intensity of a beam of photons at its passage through a particular substance or medium.

When radiation of intensity ($_0\varphi$) is incident on material of thickness (t(nm)) the transmitted intensity (ϕ) is given by Lambert-Beer-Bouguer's law [82]:

$$\phi_0 = \varphi \exp(-\alpha t) \tag{2.4}$$

For pure absorption, the constant (α) is the absorption coefficient. For scattering, obeying by Lambert-Beer-Bouguer's law, (α) is the scattering coefficient. And for the total attenuation including both is the extinction coefficient given by the sum of the absorption and scattering coefficient.

The transmittance (T) and the absorbance (A) are defined as follows [83]:

$$T = \phi|\phi_0 = \exp(-\alpha t) \tag{2.5}$$

$$A = -\log_{10}(T) \tag{2.6}$$

A relation between transmittance (T), spectral absorbance (A) and spectral reflectance (R), according to the law of conservation of energy is given by [84]:

$$\boldsymbol{T + R + A = 1} \tag{2.7}$$

Based on the equations (2.5) we can obtain the following expression of absorption coefficient [[83]-[85]]:

$$\boldsymbol{\alpha = -\frac{\ln(T)}{t} \approx 2.303\frac{A}{t}} \tag{2.8}$$

We are using equation (1.14) for calculating the reflectance and equation (2.6) for calculating the absorption coefficient in this work.

For ($\boldsymbol{hv < E_g}$), no electron hole pairs can be created, the material is transparent and ($\boldsymbol{\alpha}$) is small. For ($\boldsymbol{hv > E_g}$) absorption should be strong and it is clear that ($\boldsymbol{\alpha}$) must be strong. The absorption coefficient ($\boldsymbol{\alpha}$) is related to the incident photon energy (hv) and the optical band gap energy of the material as [[81], [85]]:

$$\boldsymbol{(\alpha hv) = C(hv - E_g)^n} \tag{2.9}$$

Where C is a constant is a constant depending upon the transition probability,$\boldsymbol{E_g}$ is the optical band gap, it is shown in figure 2.18, it is the separation energy between bottom of the conduction band and top of the valence band. (hv) is the photon energy, where (v) is the frequency of the incident photon, (h) is the Planck's constant and (n) is a constant it is equal to 1/2 or 3/2 depending on whether transition is allowed or forbidden.

For allowed direct transitions (n=1/2) and for allowed indirect transition (n=2). Thus if the plot of $\boldsymbol{(\alpha hv)^2}$ against hv is linear then the transition is direct allowed [82].

From the calculated absorption coefficient ($\boldsymbol{\alpha}$) values the extinction coefficient (k) of

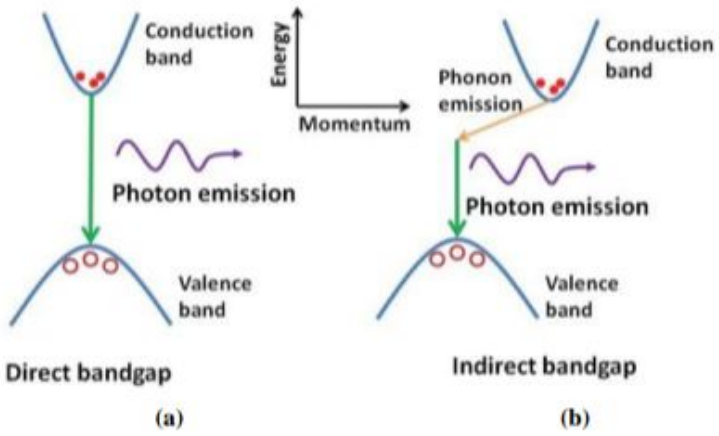

Figure 2.20: Direct (a) and indirect (b) band gap [85].

the films were calculated over visible and near infra-red wavelengths using the following formula [86]:

$$k = \frac{\alpha\lambda}{4\pi} \tag{2.10}$$

Where λ is the wavelength of the incident photon.

The rise and fall in the extinction coefficient are directly related to the absorption of light. In the case of polycrystalline films, extra absorption of light occurs at the grain boundaries [85]. This leads to non-zero value of k for photon energies smaller than the fundamental absorption edge.

B. **Energy band gap:**

The energy band gap and transition type can be determined from mathematical treatment of data obtained from optical transmittance versus wavelength. According to Tauc's relation for direct bang gap semiconductor such as NiO [[85], [86]]:

$$(\alpha h\upsilon)^2 = A(h\upsilon - E_g) \tag{2.11}$$

Where (A) is a constant, (E_g) is the optical gap energy. Figure 2.19 shows the plot of $(\alpha h\upsilon)^2$ versus (hv), it reveals the linear nature of the plot near absorption edge indicates the existence of the direct transition between bands. Hence, this linear relationship is a clear indication that the material is direct band gap semiconductors.

Extrapolating the straight line portion of the absorption spectrum in figure 2.19 intersects the zero absorption coefficients ($\boldsymbol{\alpha = 0}$) (energy axes) [87]. The value of energy at this interesting point indicates the energy of band ($\boldsymbol{E_g}$).

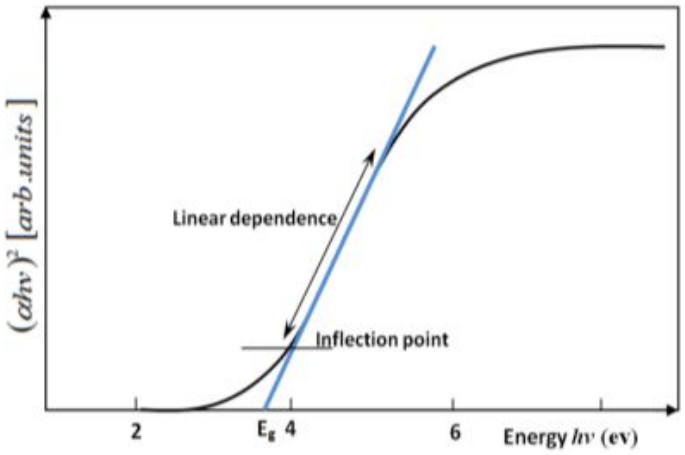

Figure 2.21: Determination of the energy gap Eg by the extrapolation method from the variation of $\boldsymbol{(\alpha hv)^2}$ as a function of hv for a thin layer. [86]

C. **Urbach energy:**

Mott and Dais noted that oppositely to pure crystalline structures, where the fundamental edge is mainly determined by conduction and valence levels, ion-doped binary semiconductor compounds present a particular optical absorption edge profile.

In these materials, the absorption coefficient profile increases exponentially with the photon energy beneath the energy gap. This variation results in "blurring" of the valence conduction bands and narrows slightly the band gap by the occurrence of the so called Urbach tails (figure 2.20).

Urbach tailing has been attributed, to various causes. Earliest investigations tried to relate it to the thermally induced lattice disorder [[88], [89]]. Generally, at optical absorption, near band edges, an electron from the top of the valence band gets excited to the bottom of the conduction band across the energy band gap. During this transition process, if these electrons encounter disorder, it causes changing in density of their states $\boldsymbol{\xi(hv)}$, tailing into the energy gap. This tail of $\boldsymbol{\xi(hv)}$ extending into the energy band gap is termed as Urbach tail. Consequently, absorption coefficient $\boldsymbol{\alpha(hv)}$ also tails off in an exponential manner and the energy associated with this tail is referred

to as Urbach energy and can be calculated by the following equation :

$$\boldsymbol{\alpha = \alpha_0 \exp(\frac{hv}{E_u})} \tag{2.12}$$

$$\boldsymbol{\ln \alpha = \frac{1}{E_u}(hv) + \ln \alpha_0} \tag{2.13}$$

Where ($\boldsymbol{\alpha_0}$) is the pre-exponential factor, (hv) the photon energy and ($\boldsymbol{E_u}$) is the band tail width commonly called Urbach energy. The band tail width is also related to the disorder in the film network [[89], [90]]. The Urbach energy, or the disorder, can be estimated from the inverse slope of the linear plot of $\boldsymbol{\ln(\alpha)}$ versus (hv) as represented in Figure 2.20.

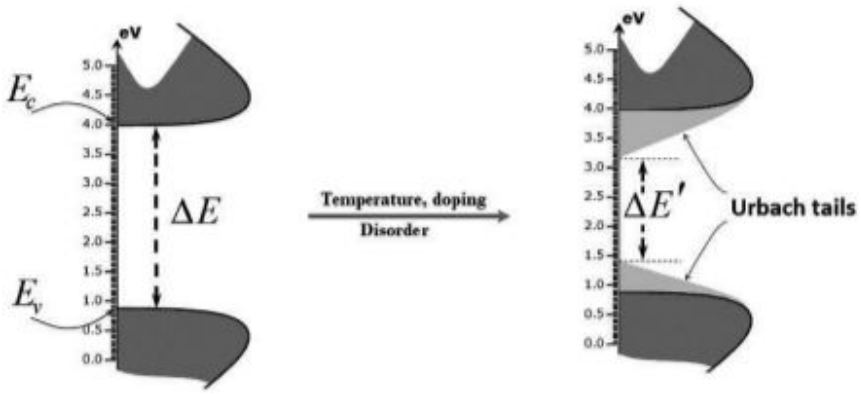

Figure 2.22: Schema of Urbach tails [88].

2.4.3 Electrical characterization

Electrical characterization methods for the analysis of thin films include the measurement of the electrical resistivity ($\boldsymbol{\rho}$). $\boldsymbol{\rho}$ is a key physical property of all materials. It is often necessary to accurately measure the value of $\boldsymbol{\rho}$ of a given material.
There are four methods commonly used for the measurement of resistivity such as:

a) Direct method

b) Two point probe method

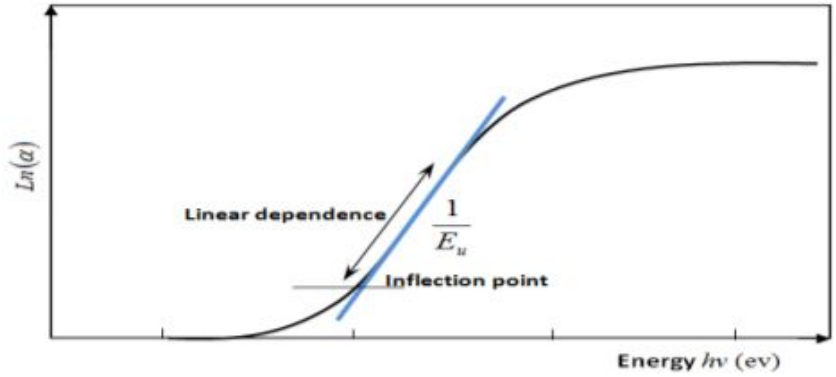

Figure 2.23: determination of the Urbach energy from the variation of ln ($\boldsymbol{\alpha}$) as a function of hv for a thin layer [90].

***c*)** Four point probe method

***d*)** Van der Pauw method

In this work, four point probe method has been used for electrical measurements.

Four Point Probe Method

The four point probe method has proven to be a convenient tool for the resistivity measurement of small size (of the order of mm) specimen. This method is applicable when the distance between the probes is small compared to the smaller dimension of the sample, and provided none of the probe is too close to an edge of the sample.

Resistivity measurement using the four-point technique

Four metal spikes are applied to the sample. The probe is comprised of four contacts that are arranged in a linear fashion and are evenly distributed. The source supplies an electric current, denoted as I, which flows via the external terminals. The voltage V is measured across the terminals of the two inner tips.

The resistivity is linked to the measurement of the $\frac{\boldsymbol{\Delta V}}{\boldsymbol{I}}$ ratio according to the relationship :

$$\boldsymbol{\rho = \frac{\Delta v}{I}.e.\frac{\pi}{\ln 2}} \tag{2.14}$$

The square resistance of a layer is defined by the resistance of a sample whose length is equal to the width. In the case of a uniformly doped layer [[96],[96]], the sheet resistance $\boldsymbol{R_D}$ of a

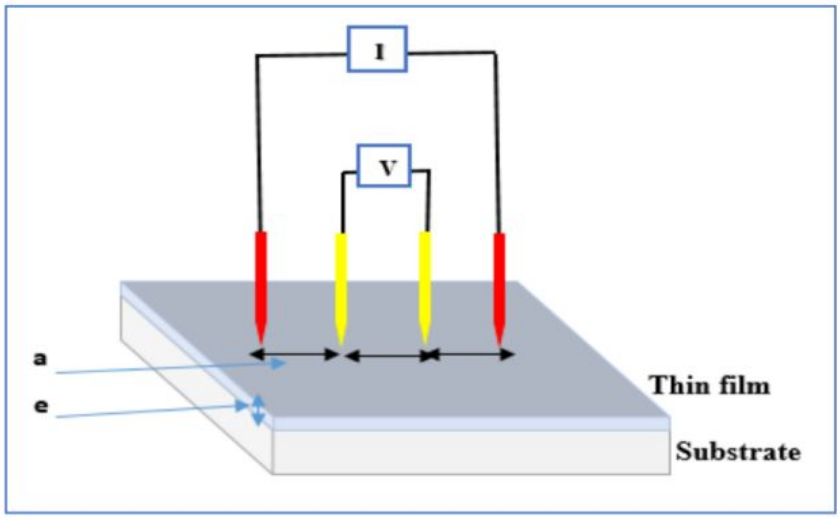

Figure 2.24: Diagram showing how to measure resistance using four-point method.

layer of thickness e is linked to the resistivity $\boldsymbol{\rho}$ by the relationship :

$$\boldsymbol{R_D = \frac{\rho}{e}} \tag{2.15}$$

with $\boldsymbol{\rho}$ the film resistivity and e the film thickness.

CHAPTER

3

EXPERIMENTAL PROCEDURES AND RESULTS

3.1 Experimental device used

We deposited CuO thin films by spray pyrolysis method on cleaned glass substrates. The assembly was carried out at the LRPCSI laboratory of the University of Skikda.

The device used is very simple, it is a manual sprayer, in which, we put the deposition solution which is in our case copper chloride $\boldsymbol{CuCl_2}$, the latter is doped with lithium with a percentage of $\mathbf{2\%, 4\%}$, and $\mathbf{6\%}$ using the lithium chloride solution LiCl , the sprayer is fixed at a distance of 25 cm from the substrate, the nozzle of the latter is oriented towards the heated substrate, the temperature of the heating plate is displayed by a thermometer from a thermocouple laid on the substrate. The block diagram of the deposition system used is shown in Figure (3.1).

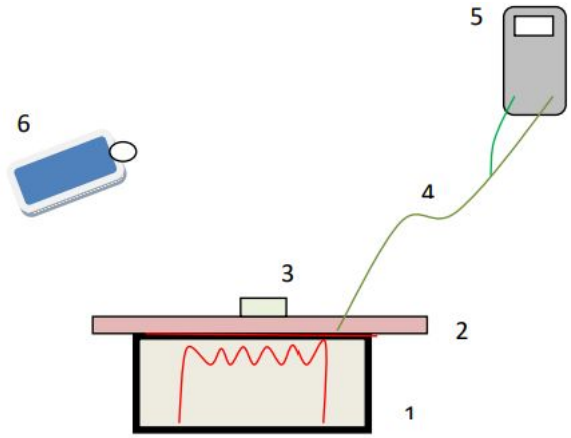

Figure 3.1: Diagram of the thin film deposition device by pyrolysis spray technique.

Figure 3.2: Actual mounting of the pyrolysis spray mounted at the LRPCSI laboratory at the University of Skikda.

Figure 3.3: The dehydrated copper chloride doped Li solution used for the deposition of our layers.

Figure 3.4: Actual photo of thin films obtained from copper oxide CuO.

The solution	$(CuCl_2.H_2O) + (LiCl.H_2O)$
The molarity of two solutions	0.1 mol/l
Substrate	Verre
Substrate temperature	$350° \pm 5°C$
The bec-substrate distance	25 cm
The bec-substrate angle	$45°$
Time of spray	1s
Time between two sprays	1s
Spray number	100

Table 3.1: Experimental conditions for the elaboration of Li-doped CuO thin films.

3.2 Filing procedure

CuO will be deposited on glass substrates that are cut by a diamond tip pen. Taking into account that the quality of the deposit depends on the propretity and the surface condition of the substrate, the latter are cleaned with acetone, after rinsing with distilled water and finally drying with a dryer.

To obtain the copper oxide films CuO doped Li, we sprayed a copper chloride solution $(CuCl_2.H_2O)$ by mixing with the LiCl lithium chloride solution on a glass substrate heated to $350°C$ with a percentage of 2%, 4% , and 6%.

The following table (3.1) groups the parameters used when filing:

3.3 Identification of the material obtained

The comparison of the data with the JCPDS references (sheet N=45-0937) confirmed the cassiterite structure (monoclinic structure) of our films. The CuO phase was obtained around $2\theta = 36.43°, 38.51°, 47.33°, 54.58°, 58.77°, 63.13°, 66.22°$ and $68.12°$ which corresponds respectively to the planes (002), (111), (-202), (020), (202) , (-113) , (312) and (113). (Figure 3.5).

Diffraction spectra show that our material has a polycrystalline structure. In all these films there are two preferential directions in the directions (-111) and (002) the latter which is the most intense. The intensity of these two peaks increases with the increase in the doping rate (Figure 3.5).

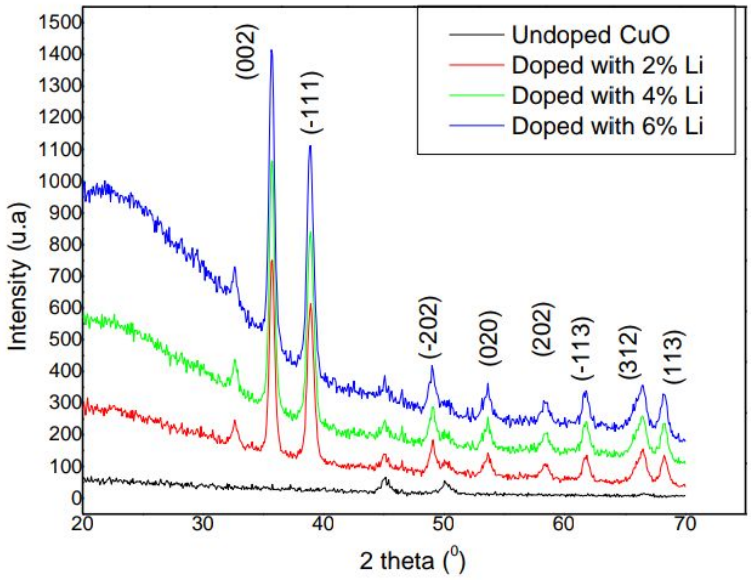

Figure 3.5: Diaffractograms of Li-doped CuO layers for different doping rates

The texture coefficients are calculated from the XRD data by using the equation [98]:

$$\boldsymbol{TC_{(hkl)} = (I_{(hkl)}/I_{0(hkl)})/\left(1/N\sum_{N}(I_{(hkl)}/I_{0(hkl)})\right)} \tag{3.1}$$

Where $\boldsymbol{I_{0(hkl)}}$ is the standard relative intensity, $\boldsymbol{I_{(hkl)}}$ is the measured intensity and Nis the number of reflections. The texture coefficients of (002) and (-111) planes were calculated and their changes with increasing Li-doping. It was observed that the texture coefficient of the (002) plane was greater than unity which decreased with increasing doping rate up to **2%** of Li and stabilize around to unity . It is known that an enhancement in the texture coefficient denotes increased number of grains along the plane. Therefore, it can be concluded that the Li-doping reduces the number of grains at low concentrations, but increases it again at high concentrations. It is also clear that (002) is the preferential orientation for Li-doped CuO films compared to the pure CuO. Naveena et al [99] and Parabu et al [100] also reported in their studies that the (002) plane is the preferential orientation of the CuO films.
The crystallite sizes, D, of the films were obtained from the two inten sepeaks using the Debye–Scherer equation [101]:

$$\boldsymbol{D = \frac{0.89\lambda}{\beta\cos\theta}} \tag{3.2}$$

Where $\boldsymbol{\lambda = (1.54056)}$ is the wavelength, $\boldsymbol{\theta}$ is the Bragg's angle of the peaks, $\boldsymbol{\beta}$ is the FWHM. The crystallite size of the samplesis influenced by the Li concentration as shown in Figure 3.3.The average crystallite size $\boldsymbol{(D_{mean})}$ values are found to be 124, 112, 114 and $\boldsymbol{104\mathring{A}}$ for 0, 2, 4 and $\boldsymbol{6\%}$ Li-doped films, respectively. As can be seen from the structural parameters listed in Table 1 and Figure 3.5, the Li-doping caused larger crystallites to form. The dislocation density ($\boldsymbol{\delta}$)and the strain ($\boldsymbol{\varepsilon}$) were obtained using the equations [5]:

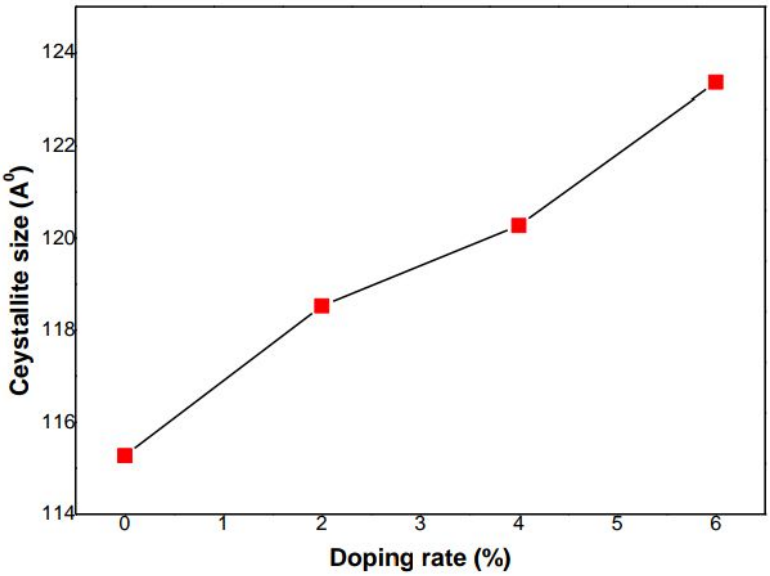

Figure 3.6: Plot of crystallite size of Li-doped CuO layers for different doping rates

$$\boldsymbol{\delta = \frac{1}{D^2}} \tag{3.3}$$

$$\boldsymbol{\varepsilon = \frac{\beta \cos \theta}{4}} \tag{3.4}$$

$\boldsymbol{\varepsilon}$ and $\boldsymbol{\delta}$ values belonging to (002) plane are given in Table 3.2. As can be seen, the Li-doping caused a slight decrease in both parameters. Moreover an inversely proportional relationship between strain and size of the crystallites was observed.$\boldsymbol{\varepsilon}$ and $\boldsymbol{\delta}$ values are enhanced due to the increase in the number of grainsand decrease in crystallite with Li-doping. This change can also be explained by the difference in the ionic radii between $\boldsymbol{Li^{+}(0.76\mathring{A})}$ and the copper $\boldsymbol{Cu^{2+}(0.73\mathring{A})}$ ions. Similar results comparable to those obtained here were also found by Shannonet al.[103]. However, attenuated strain suggests there diction in the lattice

Li Concentrations (at.%)	$\mathbf{2\theta(°)}$	FWHM	$\boldsymbol{d_{hkl}(\AA)}$	$\boldsymbol{D(\AA)}$	$\boldsymbol{\varepsilon()}$	$\boldsymbol{\delta(1/nm^2)10^{-3}}$
0	35.96	0.676	2.497	115.272	0.31	7.5257
2	35.97	0.307	2.498	118.526	0.41	7.1181
4	35.98	0.451	2.498	105.272	0.66	9.0234
6	35.88	0.471	2.500	117.362	0.65	7.2601

Table 3.2: Structural parameters of Li-doped CuO thin films

Li (at.%)	$\boldsymbol{a(\AA)}$	$\boldsymbol{b(\AA)}$	$\boldsymbol{c(\AA)}$
0	4.643	3.412	5.112
2	4.643	3.406	5.101
4	4.671	3.402	5.118
6	4.641	3.409	5.095
JCPDS : N=45-0937	4.653	3.410	5.108

Table 3.3: Lattice constants for CuO the films pure and Li-dopedCuO.

defects concentration. Accordingly, to the fact that these two quantities are related to the dislocation networks, their decrease is synonym of better crystalline quality. This means that the doped films haves maller micro stain values, which may denote a slight enhancement in the crystallinity. Similar conclusion supporting this effect was also reported by Bayansalet al. [104].

The lattice parameters a, b, c for a monoclinic structure are evaluated using this equation:

$$\frac{\mathbf{1}}{\boldsymbol{d^2_{hkl}}} = \frac{\mathbf{1}}{\mathbf{sin^2}\,\boldsymbol{\beta S}}\left(\frac{\boldsymbol{h^2}}{\boldsymbol{a^2}} + \frac{\boldsymbol{l^2}}{\boldsymbol{c^2}} - \frac{\mathbf{2}\boldsymbol{hl}}{\boldsymbol{ac}}\right) + \frac{\boldsymbol{k^2}}{\boldsymbol{b^2}} \tag{3.5}$$

Where the values a, b, c denote the lattice parameters, (hkl) are the Miller indices, d is the inter planar distance and $\boldsymbol{\beta}$ is $\mathbf{99.48°}$ for the monoclinic structure. The calculated lattice constants for the films are given in Table 3.3 where the standard values of the constants, $\boldsymbol{a = 4.6530\AA, b = 3.410\AA}$ and $\boldsymbol{c = 5.1080\AA}$ were used (JCPDS file no: N=45-0937). It is obvious that the constants calculated in this study are very close to the standard values. This might be due to the variation of the lattice constants by the fact that CuO has a complex monoclinic structure, and the strains that occurred during the formation of the films. However, the increase in Li concentration led to a slight increase in the lattice constants. At **4%** of Li-doping the lattice constant, a, reached $\mathbf{4.671\AA}$. The observed increase in the parameter a can be attributed to the different ionic radii of $\boldsymbol{Cu^{2+}}$and $\boldsymbol{Li^{+}}$.

3.4 Characterization by -Raman spectroscopy

In Figure 3.7, we have represented the Raman spectra of CuO films for different doping rate. Raman spectra are composed of three main modes Ag and 2 Bg located at $\mathbf{277.27}\boldsymbol{cm}^{-\mathbf{1}}$, $\mathbf{333.11}\boldsymbol{cm}^{-\mathbf{1}}$ and $\mathbf{624.64}\boldsymbol{cm}^{-\mathbf{1}}$. These peaks are widely reported in the literature [[105]-[107]]. This confirms the presence of a single CuO phase with a monoclinic structure as deduced from the diffraction analysis. Our Raman spectra were recorded using a Bruker senterra Raman spectrometer with a 532 nm Laser AlGaAs excitation. There is also a

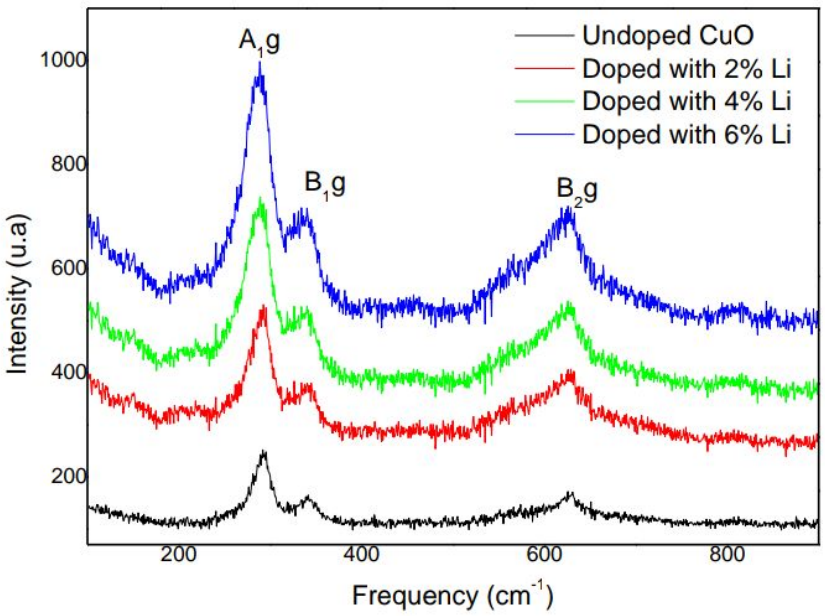

Figure 3.7: CuO Raman spectrum for different flow rates.

high intensity of the Ag mode, It is well known that this Raman mode which characterizes the monoclinic structure in a single CuO phase. Ag's peak position is highly dependent on several factors such as grain size and film crystallinity [[108],[109]]. From the obtained results we notice that films have better structural properties of our CuO layers.

3.5 Thickness measurement

The thickness of our layers was measured by the profilomer with mechanical probe, in our case we find a thickness of 486 nm, which corresponds to a fixed spray number of 100 spray (optimal spray : a number that has high optical, structural and electrical characteristics).

3.6 Electrical properties

The electrical properties of thin films are of considerable interest in several applications such as solar cells, gas collectors and flat screens. Among these properties we cite electrical resistivity as one of the most important parameters in the study of transparent and conductive oxides. For the calculation of the resistances of our films, we used a device measuring by four points, model JANDEL connected to a Keithley 2400 metric source (Figure 3.8).

Figure 3.8: Real image of Keithley 2400.

The electrical resistivity is plotted as a function of the doping rate of Li.

Therefore, the resistivity of the films was measured at room temperature in the dark using the four probe method. Figure 3.9 shows the variation of the resistivity of the films with respect to Li concentration. The results reveal that the resistivity of the films decreased with increasing of Li concentration from 339 to 186 $\boldsymbol{K\Omega}$. The decrease in resistivity might be due also to these reasons: (i) improved crystallization, (ii) interstitial position of Li ionsand (iii) reduction in the carrier scattering as a consequence of the decrease in the number of grains. Anand et al. [110] and Khodair et al. [111] reported comparable results to resistivity values calculated in this study.

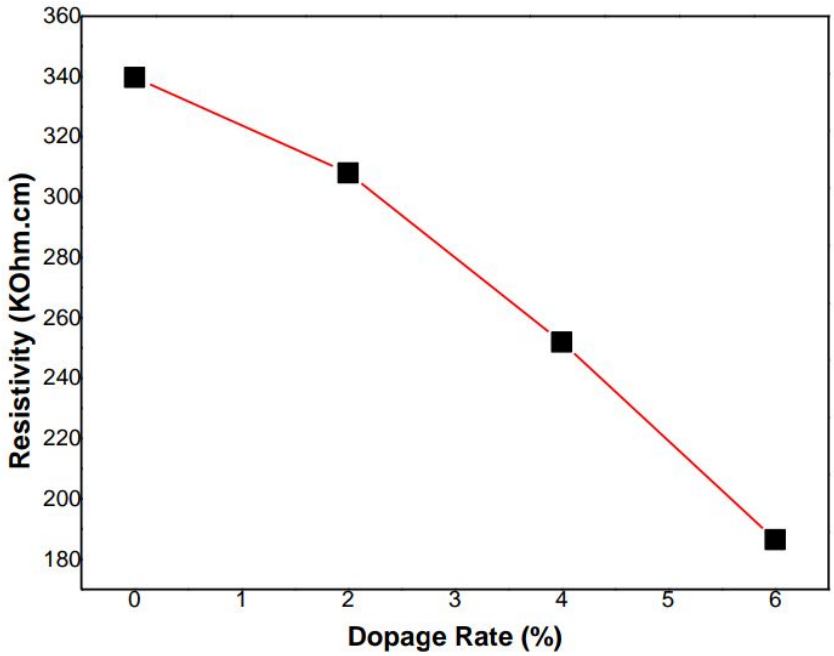

Figure 3.9: Variation in electrical resistivity of CuO layers as a function of Li doping rate.

3.7 UV-Visible Optical Caraterisation

3.7.1 Transmission

Optical transmission in the UV-visible domain is an important characterization to assess the quality of deposited films. It must embrace maximum in visibe [15-20]. The transmission spectra are obtained by UV spectrophotometer – visible Shimatzu 1700 (Figure 3.10), in the wavelength range between 200-900 nm. The results are shown in Figure 3.11.

*

Figure 3.10: Real image of UV spectrophotometer – visible Shimatzu 1700.

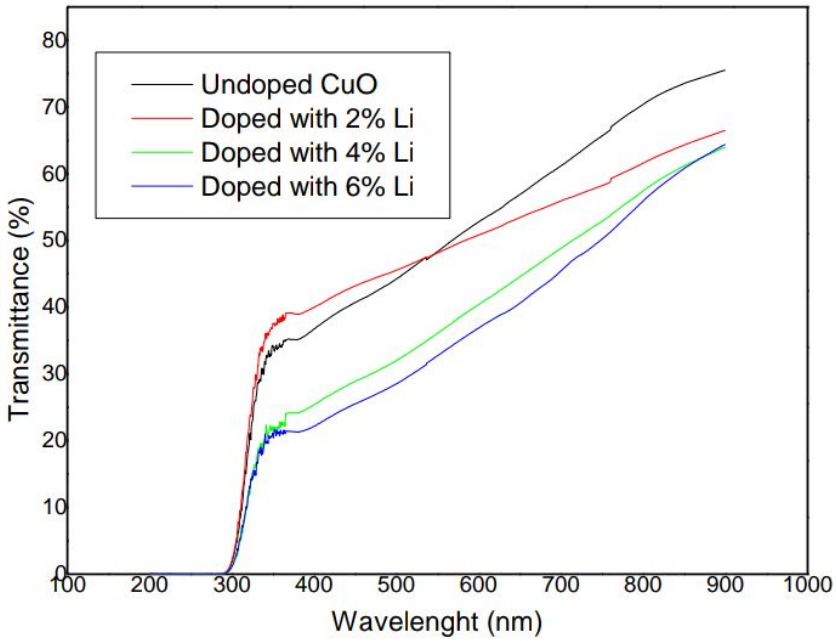

Figure 3.11: Visible UV transmission spectrum of CuO for different percentage of doping by Li.

Figure 3.12 the optical transmittance with respect to the wavelength in the spectral range from 300 to 900 nm. The spectrum of undoped film exhibited a maximum (about 70%) around 780 nm. On the other hand, it was decreased with increasing Li-doping and reached a minimum (about 60%) when Li concentration was to 6 at.%. This range of transparency corresponds to an acceptable absorption in CuO due to the transitions between the valence and the conduction band. The decrease in the transmittance originates from the increase in the surface roughness of the films.Similar results are outlined by Naveena et al. and Hussin et al. [[118], [119]].

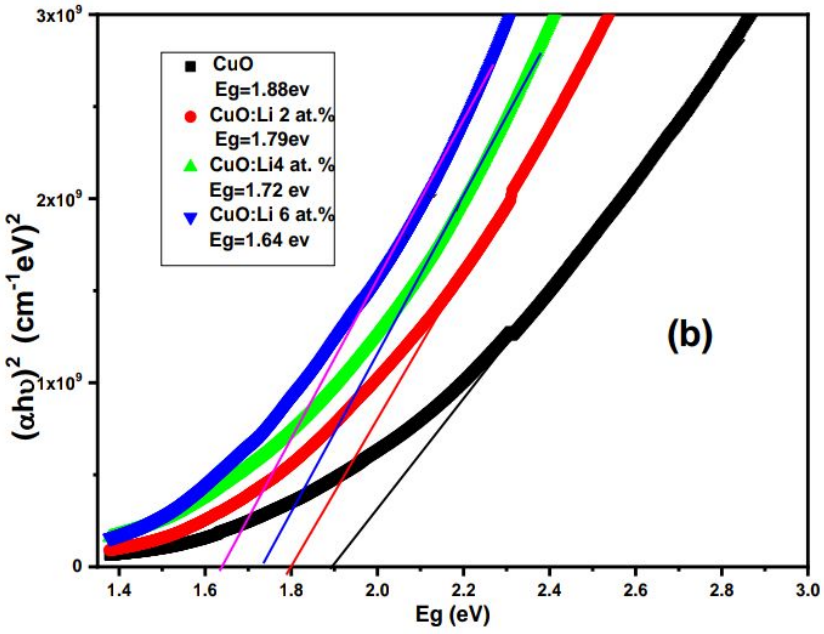

Figure 3.12: Band gap variation of the films CuO pure and Li-doped CuO.

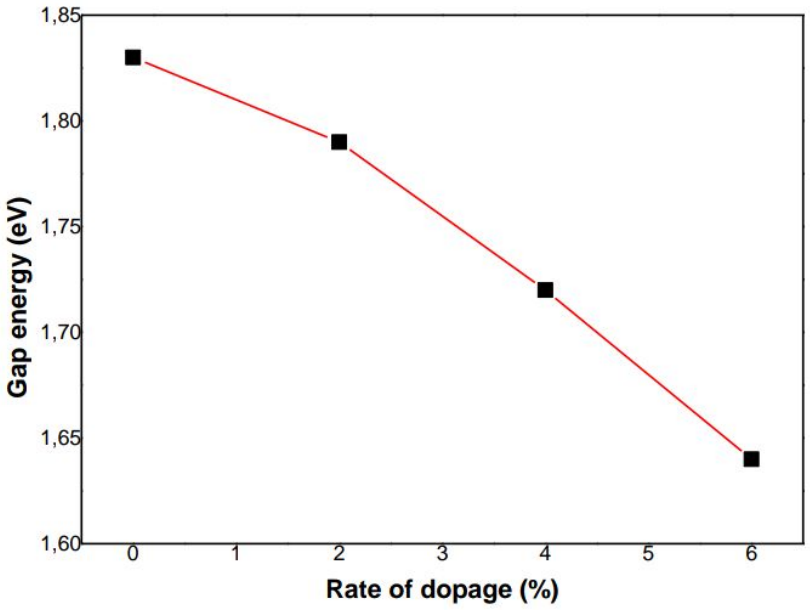

Figure 3.13: Behavior of direct band gap energy of the films with respect to the Li concentration.

To obtain the E_g values, Tauc plots which shows the variation of $(ahv)^2$ with respect to the photon energy (hv) was drown. The E_g values were obtained by extrapolating the linear part and finding the interception point of the plots with the x-axis in Figure 3.12.

The estimated $\boldsymbol{E_g}$ values of the films were found to be 1.88, 1.79, 1.72 and 1.64 eV, respectively, and are shown in Figure 3.13. At increasing Li concentrations, $\boldsymbol{E_g}$ is reduced from 1.88 to 1.64 eV. Which is in good accordance with previously reported data [121]. This decrease might be attributed to variations in the crystallite size and Li ions adopting substitution position sites in the CuO lattice. When Li is doped into CuO, the optical energy band gap decreased due to band tail effects. This is because the donor density increases in parallel with the increase in the ratio of Li added to the structure. This can result in the creation of tail-like states to extend below the conduction band [121].

CONCLUSION

To improve the quality of film layers, another extremely interesting area for CuO copper oxide was to study the influence of doping. In fact, the X-ray diffraction (XRD) showed that Li's doping contents improved CuO's crystallinity without damaging its monoclinic structure. The films studied with the highest doping concentrations showed the highest percentage of transmission. However, the optical gap has been studied for different amounts of doping. Indeed, the electrical part revealed a significant increase in conductivity and mobility.

A decrease in resistivity and carrier concentration of prepared films was studied and confirmed that growth in films was p-type in nature. These results lead to experimental investigations when improving their properties for gas sensors.

In addition, the material studied CuO presented in this work is of great importance because it allows the manufacture and development of an efficient gas sensor at very low cost. In addition, it has great potential for inexpensive photovoltaic devices. Further research is needed to achieve these goals. A lot of work and effort is still underway in our laboratory to use this material to make a gas sensor and thin film based CuO photovoltaic devices. It is an ambitious task that is a perspective like a future work that will be a continuation of the present work.

BIBLIOGRAPHY

[1] Q. Xu, Y. Zhao, J.Z. Xu, J.J. Zhu, Preparation of functionalized copper nanoparticles and fabrication of a glucose sensor, Sensors Actuators, B Chem. 114 (2006) 379–386. https://doi.org/10.1016/j.snb.2005.06.005.

[2] L. Szablewski, Glucose Homeostasis – Mechanism and Defects, (2015). https://doi.org/10.5772/22905.

[3] J.F. Vetelino, A. Reghu, Introduction to sensors, Introd. to Sensors. (2017) 1–180. https://doi.org/10.1201/9781315218274.

[4] Development of a Glucose Sensor for Diabetic Patients, n.d.

[5] O.Daranfad «Elaboration et caractérisation des couches minces de Sulfure de Zinc préparées par spray ultrasonique »,mémoire magister, université Mentouri –Constantine, page12.

[6] L. Herissi « Élaboration et caractérisation de couches minces d'oxydes métalliques destinées à des applications optoélectroniques » thèse doctorat, Université Larbi Ben M'hidi -Oum El Bouaghi, 2016, page 4.

[7] M.Ayachi «Elaboration par la méthode sol gel spin coating et caractérisations des couches minces de ZnO »mémoire magistère, université Jijel, 2012, page6.

[8] J.E. Greene, Chapter 12: Thin film nucleation, growth, and microstructural evolution: An atomic scale view, Science, Applications and Technology, (2010) 554.

[9] K. Wasa, M. Kitabatake, H. Adachi, Thin film materials technology-Sputtering of Compound Materials, William Andrew publishing 1 (2004) 102.

[10] https://www.cefi.org (Fra DESS.old / dess$_2$65$html$).$S.Yamaga$, $A.Yoshokawa$, $H.Kasain$,

[11] I.C. Ndukwe, Sol. Energy Mater. Ground, Cells 40 (1996).

[12] T.E. Varitimos, R.W. Tustison, thin Solid Films 151 (1987).

[13] L.V. Devi, S. Sellaiyan, S. Sankar, K. Sivaji, Structural and optical investigation of combustion derived La doped copper oxide nanocrystallites, Materials Research Express, 5 (2018) 024002.

[14] C.R. Gobbiner, G.R. Dillip, S.W. Joo, D. Kekuda, Heterogeneity of photoluminescence properties and electronic transitions in copper oxide thin films: A thickness dependent structural and optical study, Ceramics International, 44 (2018) 16984-16991.

[15] E. C. Nwanna, P. E. Imoisili, S. O. Bitire, et T. Jen, « Biosynthesis and Fabrication of Coppe Oxide Thin Films as a P-Type Semiconductor for Solar Cell Applications », Coatings, vol.11, 2021.

[16] S. Using et S. Pyrolysis, « Structural and Optical Properties of CuO Thin Films Synthesized Using Spray Pyrolysis Method », , Coatings, vol.11, 2021.

[17] R. U. Osuji, F. I. Ezema, D. S. Polytechnic, et D. State, « Synthesis and Characterisation of Copper Oxide Thin Films Using Successive Ionic Layer Adsorption Reaction (SILAR) Method », p. 68-76, 2016.

[18] M.Lamri Zeggar, «Cupric Oxide thin films deposition for gas sensor application», Doctorat thesis, frères Mentouri Constantine 1 university, Algeria, 2016.

[19] P.K.Ooi, S.S. Ng, M.J. Abdullah, H. Abu Hassan, Z. Hassan, Materials Chemistry and Physics 140 (2013) 243.

[20] .A .Ezenwa, Chem. Phys, 50 (2012) 41.

[21] S. C. Ray, Solar Energy Materials Solar Cells 68 (2001) 307.

[22] A. Chapelle, « Elaboration et caractérisation de films minces nano composites obtenus par pulvérisation cathodique radiofréquence en vue de leur application dans le domaine des capteurs de CO2 », thèse doctorat, université Toulouse, 2012, page 40.

[23] F.Z.Chafi, «Deposition of undoped and doped Copper Oxide thin films by Spray Pyrolysis technique: Experiment and Theory », doctoral thesis, University Mohammed V, Rabat, 2017,page22.

[24] A.Bejaoui, « Capteurs à base des couches minces d'oxyde de cuivre (II) (CuO) : Optimisation et modélisation en vue de la détection de gaz », thèse doctorat, université de Carthage, 2013, page 26 ,27.

[25] S.Mechdjebi, «La synthèse des nano poudres de CuO avec la méthode précipitation Sol-Gel en utilisant le précurseurCuSO4 et l'étude de leurs propriétés structurales et optiques », mémoire magister, université Mentouri –Constantine, 2015, page29, 30.

[26] M. Kidwai, S. Bhardwaj, R. Poddar, C-Arylation reactions catalyzed by CuO- nanoparticles under ligand free conditions, Beilstein journal of organic chemistry, 6 (2010) 35.

[27] E. Barrera-Calva, J. Mé, M. Ortega-Ló, L. Huerta-Arcos, J. Morales-Corona, R. Olayo-Gonzá, Silica-copper oxide composite thin films as solar selective coatings prepared by

dipping sol gel, Advances in Materials Science and Engineering, Volume 2008, Article ID 190920,5pages(2008).

[28] K. Nagase, Y. Zheng, Y. Kodama, J. Kakuta, Dynamic study of the oxidation state of copper in the course of carbon monoxide oxidation over powdered CuO and Cu2O, Journal of Catalysis, 187 (1999) 123-130.

[29] D. Dadoo, production et application des nanostructures d'oxyde de cuivre, thèse doctorat, Université de trento- Italie, 2010.

[30] G. Papadimitropoulos, N. Vourdas, V. E. Vamvakas, et D. Davazoglou, « Optical and structural properties of copper oxide thin films grown by oxidation of metal layers », Thin Solid Films, vol. 515, no 4, p. 2428-2432, 2006.

[31] S. Choudhary et al., « Oxidation mechanism of thin Cu films: A gateway towards the formation of single oxide phase », AIP Adv., vol. 8, no 5, 2018.

[32] F.Z.Chafi, «Deposition of undoped and doped Copper Oxide thin films by Spray Pyrolysis technique: Experiment and Theory », doctoral thesis, University Mohammed V, Rabat, 2017,page22.

[33] K. Han et M. Tao, « Electrochemically deposited p-n homojunction cuprous oxide solar cells », Sol. Energy Mater. Sol. Cells, vol. 93, no 1, p. 153-157, 2009.

[34] M.Zeggar, «Cupric Oxide thin films deposition for gas sensor application », doctoral thesis, university Mentouri –Constantine, 2016, page14, 28.

[35] S. T.c and A. B. Saptarshi De a, N. Venkataramani a, Shiva Prasad b, R. O. Dusane a, Lionel Presmanes c, Y. Thimont c, P. Tailhades c, Valérie Baco-Carles c, Corine Bonningue c, « Ethanol and References 121 Hydrogen gas-sensing properties of CuO–CuFe2O4 nanostructured thin films », Power Eng., no July, 2003.

[36] L. Presmanes et al., « Integration of P-Cuo thin sputtered layers onto microsensor platforms forgas sensing », Sensors (Switzerland), vol. 17, no 6, 2017.

[37] A. Sharma, Y. Kumar, et P. M. Shirage, « Structural, optical and excellent humidity sensing behaviour of ZnSnO3 nanoparticles: effect of annealing », J. Mater. Sci. Mater. Electron., vol. 29, no 13, p. 10769-10783, 2018.

[38] N. D. Khiavi, R. Katal, S. K. Eshkalak, S. Masudy-Panah, S. Ramakrishna, et H. Jiangyong, « Visible light driven heterojunction photocatalyst of CuO-Cu2O thin films for photocatalytic degradation of organic pollutants », Nanomaterials, vol. 9, no 7, 2019.

[39] L. Sun et al., « Nitrogen-Doped Carbon-Coated CuO-In2O3 p–n Heterojunction for Remarkable Photocatalytic Hydrogen Evolution », Adv. Energy Mater., vol. 9, no 48, p. 1-11, 2019.

[40] W. Mohsen, M. A. Sadek, et H. A. Elazab, « Green synthesis of copper oxide nanoparticles in aqueous medium as a potential efficient catalyst for catalysis applications », Int. J. Appl. Eng. Res., vol. 12, no 24, p. 14927-14930, 2017.

[41] A. A. Al-Ghamdi, M. H. Khedr, M. Shahnawaze Ansari, P. M. Z. Hasan, M. S. Abdel-Wahab, et A. A. Farghali, « RF sputtered CuO thin films: Structural, optical and photo-catalytic behavior », Phys. E Low-Dimensional Syst. Nanostructures, vol. 81, p. 83-90, 2016.

[42] K. Sahu, A. Bisht, A. Dutta, T. Som, et S. Mohapatra, « Morphological, optical, catalytic and photocatalytic properties of RF magnetron sputtered Au-Cu2O-CuO nanocomposite thin films », Surfaces and Interfaces, vol. 26, no July, p. 101436, 2021.

[43] Y. Chang, M. Zhang, L. Xia, J. Zhang, G. Xing, The toxic effects and mechanisms of CuO and ZnO nanoparticles. Materials 5 (12): 2850–2871, in, 2012.

[44] R. Foudil, Thèse de magister, Université de M'sila, 2009.

[45] A. Aldrin, Preparation and characterization of certain II-VI, I-III-VI2 semiconductor thin films and transparent conducting oxides, PhD thesis, Cochin University, India-2004.

[46] F. Ynineb, Contribution à l'élaboration de couches minces d'Oxydes Transparents Conducteurs (TCO), Magister Memory, Mentouri Brother University, Constantine-2010.

[47] K.C. Sanal, Development of p-type transparent semiconducting oxides for thin film transistor applications, PhD thesis, cochin university of science and technology, (2014).

[48] Saâd Rahmane, thèse de Doctorat, Elaboration et caractérisation de couches minces par spray pyrolyse et pulvérisation magnétron, Université Mohamed Kheider– Biskra, Algérie, (2008).

[49] https://www.researchgate.net/figure/10-Cathodic-sputtering-accelerated-Ar-ions- extract atoms-from-the-target$_{f}ig9_{2}78637056[accessed16May, 2020].KhachabHamid, thèsedeDocto$ $BekrBelkaid - Tlemcen, Algérie, (2010).$

[50] Gabriel Tourbot, thèse de Doctorat, Croissance par épitaxie par jets moléculaires et détermination des propriétés structurales et optiques de nano fils InGaN/GaN, Université de Grenoble, France, (2012).

[51] Taabouche Adel, thèse de Doctorat, Etude structurale et optique de films minces ZnO Elaborés par voie physique et/ou chimique, Université Frères Mentouri Constantine I, Algérie, (2015).

[52] K. Badeker, Annalen der Physik 327, 749-66.

[53] C.M. Wang, C.Y. Wen, Y.C. Chen, K.S. Kao, D.L. Cheng, C.H. Peng, Effect of deposition temperature on the electro chromic properties of electron beam-evaporated WO3 thin films, Integrated Ferroelectrics, 158 (2014) 62-68.

[54] Esteban Martinez-Guerrero, thèse de Doctorat, Elaboration en Epitaxie par Jets Moléculaires des Nitrures d'éléments III en Phase Cubique, Institut National des Sciences Appliquées de Lyon, France, (2002).

[55] Maria Magdalena Şovar, thèse de Doctorat, du tri-iso propoxyde aux oxydes d'aluminium par dépôt chimique en phase vapeur : procédé, composition et propriétés des revêtements obtenus, INP Toulouse et Université Polytechnique de Bucarest, Romania (2006).

[56] C. Kelifi, Tin dioxide SnO2 thin films deposited by ultrasonic spray technique: Properties and applications, Doctoral Thesis, Mohamed Khider University, Biskra-2018.

[57] M. A. Aegerter, J. Puetz, G. Gasparro N. Al-Dahoudi, Versatile wet deposition techniques for functional oxide coatings, Optical Materials 26 (2004) 155.

[58] M. Othmane, Synthesis and characterization of Zinc Oxide (ZnO) Thin films deposited by spray pyrolysis for applying: electronics and photonics, Doctoral Thesis, Mohamed Khider University, Biskra-2018.

[59] G. Srinivasan, N. Gopalakrishnan, Y. S. Yu; R. Kesavamoorthy, J. Kumar, Influence of post-deposition annealing on the structural and optical properties of ZnO thin films prepared by sol–gel and spin-coating method, Superlattices and Microstructures 43 (2008) 112.

[60] https://str.llnl.gov/str/May05/Satcher.html, Novel Materials from Sol-gel Chemistry, Lawrence Livermore National Laboratory, 2005.

[61] L. Holland, Vacuum deposition of thin films. First Edition, Published 1956 by Wiley Sons.

[62] R. Zamiri, B. Singh, D. Dutta, A. Reblo, J. Ferreira, Electrical properties of Ag-doped ZnO nano-plates synthesized via wet chemical precipitation method, Ceramics International 40 (2014) 4471.

[63] S. Guellati, C. Boussahla, Étude de l'effet de dopage par nickel et du recuit sur les propriétés des couches minces d'oxyde de cuivre, Master Memory, Larbi Tebessi University, Tebessa-2019.

[64] A. Ashok, G. Regmi, S. Velumani, Growth of In2Se3 thin films prepared by the pneumatic spray pyrolysis method for thin film solar cells applications, 17th International Conference on Electrical Engineering, Computing Science and Automatic Control (CCE), Mexico, 2020.

[65] L. Hadjeris, L. Herissi, M. Assouar, T. Easwarakhanthan, J. Bougdira, N. Attaf and M S. Aida, Transparent and conducting ZnO films grown by spray pyrolysis, Semiconductor Science and Technology 24 (2009) 035006.

[66] V. K. Singh, « Thin Film Deposition by Spray Pyroysis Techniques », Emerg. Technol. Innov. Res., vol. 4, no 11, p. 1-9, 2017.

[67] Robert Waugh M, Doctorate thesis, The Synthesis, Characterization and Application of Transparent Conducting Thin Films, University College London, (2011).

[68] V. Saravanakannan and T. Radhakrishnan, "Structural, electrical and optical characterization of CuO thin films prepared by spray pyrolysis technique", International Journal of Chem Tech Research, Vol. 6, No. 1, 306-310,(2014).

[69] A. Rahdar, M. Aliahmadb and Y. Azizi, "NiO Nanoparticles: Synthesis and Characterization", Journal of Nanostructures, Vol. 5,145-151, (2015).

[70] L. Cattin, B. A. Reguig, A. Khelil, M. Morsli, K. Benchouk and J. C. Berne 'de, "Properties of NiO thin films deposited by chemical spray pyrolysis using different precursor solutions", Applied Surface Science, Vol. 254, 5814-5821, (2008).

[71] O. Belahssen, M. Ghougali and A. Chala, "Effect of iron doping on physical properties of NiO thin films", Journal of Nano-and Electronic Physics, Vol. 10, No. 2, 1-4 ,(2018).

[72] M. Mekhnache, A. Drici, L. S. Hamideche, H. Benzarouk, A. Amara, L. Cattin, J. C. Bernede and M. Guerioune, "Properties of ZnO thin films deposited on (glass, ITO and ZnO: Al) substrates", Super lattices and Microstructures, Vol. 49, No. 5,510-518, (2011).

[73] M. V. Kumar, S. Muthulakshmi, A. A. Paulfrit, J. Pandiarajan, N. Jeyakumaran and N. Prithivikumaran, "Structural and optical behavior of thermally evaporated p-Type Nickel Oxide thin film for Solar Cell Applications", International Journal of Chem Tech Research, Vol. 6, No. 13, 5174-5177 ,(2014).

[74] M. Karunakaran, S. Maheswari, K.Kasirajan and S. Dineshraj, "Physical properties of Nanocrystalline Tin Oxide thin film by chemical spray pyrolysis method", International Journal for Research in Applied Science Engineering Technology, Vol. 4, No. 7, 691-695,(2016).

[75] A. F. Saleh, "Structural and morphological studies of NiO thin films prepared by Rapid thermal oxidation method", International Journal of Application or Innovation in Engineering Management, Vol. 2, No. 1,16-21 ,(2013).

[76] Y. Z. Dawood, M. H. Hassoni and M. S. Mohamad, " Effect of solution concentration on some optical properties of indium oxide doped with SnO2 thin films prepared by chemical spray pyrolysis technique", International Journal of Pure and Applied Physics, Vol. 2, No. 1, 1-7 ,(2014).

[77] S. Ilican, M. caglar, Y. caglar, "Determination of the thickness and optical constants of transparent indium-doped ZnO thin films by the envelope method", Materials Science-Poland, Vol. 25, No. 3,709-718,(2019).

[78] S. Benhamida, "Caractérisation Des Couches Minces D'oxyde De Nickel (NiO) Elaboré Par Spray Pyrolyse", Doctoral Thesis, Biskra University, Algérie, (2018).

[79] P. Miles, "High transparency infrared materials - A technology update", Optical Engineering, Vol. 15, 451-459, (1976).

[80] A. V. Rajgure, "Synthesis and Characterization of nano-crystalline ZnO gas sensor", Doctoral Thesis, Solapur University, India, (2014).

[81] A. Beggas, "Elaboration and characterization of chalcogenide thin films by chemical bath deposition technique", Doctoral Thesis, Biskra University, Alegria, (2018).

[82] B. A. Ezekoye and C.E. Okeke, "Optical properties in PbHgS ternary thin films deposited by solution growth method", The Pacific Journal of Science and Technology, Vol. 7. No. 2, 108-113, (2006).

[83] A. D. A. Buba and J. S. A. Adelabu, "Optical and Electrical Properties of Chemically Deposited ZnO Thin Films", The Pacific Journal of Science and Technology, Vol. 11, No. 2, 429-434, (2014).

[84] S. S. Roy and J. Podder, "Synthesis and optical characterization of pure and Cu doped SnO2 thin films deposited by spray pyrolysis", Journal of Optoelectronics and Advanced Materials, Vol. 12, No. 7, 1479 -1484, (2010).

[85] F. N. Al.Shammary, "Optical characteristics of NiO thin film on glass formed by Chemical spray pyrolysis", Journal of Kufa – Physics, Vol. 2, No. 1, 22-27, (2010).

[86] S. Sriram and A. Thayumanavan, "Structural, optical and electrical properties of NiO thin films prepared by low cost spray pyrolysis technique", International Journal of Materials Science and Engineering, Vol. 1, No. 2, 118-121, (2013).

[87] N. N. Jandow, "Effects of Cu-doping on optical properties of NiO", International Letters of Chemistry, Physics and Astronomy, Vol. 48, 155-162, (2015).

[88] K.Boubaker, "A physical explanation to the controversial Urbach tailing universality, The European Physical Journal Plus", Vol. 126, No. 10, 1-4, (2011).

[89] F. N. C. Anyaegbunam and C. Augustine, " A study of optical band gap and associated Urbach energy tail of chemically deposited metal oxides binary thin film", Digest Journal of Nanomaterial's and Biostructures, Vol. 13, No. 3, 847-856, (2018).

[90] K. Anandan and V. Rajendran, "Effect of Fe Doping in NiO Semiconductor Nanoparticles and Studies on Their Structural, Magnetic and Optical Properties: Synthesized Via the Precipitation Process", International Journal of Advanced Trends in Engineering and Technology, Vol. 2, No. 2, 1-5, (2017) .

[91] Jday Rawen , « Caractérisation microstructurale du graphite sphéroïdal formé lors de la solidification et à l'état solide » ,thèse doctorat, Université de Toulouse, 2017, page31.

[92] A. Atyraou, « Elaboration de TiO2 sous forme de couche mince dopée et nano tubulaire : caractérisation électrochimique et performance photo catalytique », thèse doctorat, université Tunis el Manar, 2013, page 58.

[93] O. A. Maslova, « Spectroscopie et imagerie Raman de matériaux inhomogènes », Thèse doctorat, université d'Orléans, 2014, page 19,20.

[94] F. Labrèche « Elaboration et caractérisation des films minces d'oxyde de titan pur et dopés Nd et Ag »thèse doctorat, université Jijel, 2018, page 45.

[95] M.C.Benachour, « Elaboration et caractérisation des couches minces de TiO2 dopées à l'erbium, à différentes températures et épaisseurs », mémoire magistère, université Mentouri -Constantine, 2011, page40, 61.

[96] M. Hellal , « Elaboration et caractérisation des couches minces nanocristallines », mémoire magistère, université Mentouri -Constantine, 2014, page 24,25.

[97] S.Yahiaoui, «L'effet de la molarité des différentes sources d'étain sur les propriétés des couches minces d'oxyde d'étain SnO2 élaborées par Spray ultrasonique », mémoire magistère, université Mohamed Kheider-Biskra, 2014, page 52.

[98] M.V. Zdorovets, D.B. Borgekov, I.E. Kenzhina, A.L. Kozlovskiy, Phys. Lett A.382, 175, 2018.

[99] B.Rahal, B.Boudine, Y.Larbah, N.Souami.J.Inorg.Organomet.Polym Materi.31, 4001, 2021.

[100] A.Badawi, M.G.Althobaiti, S.S. Alharthi, A.M. Al-Baradi, Phys. Lett A .411, 127553; 2021.

[101] R.D. Shannon, Acta. Cryst. A.32, 751, 1976.

[102] F. Bayansal, O. Sahin, H.A. Cetinkara, Thin Solid Films.697, 137839; 2020.

[103] H.A.Hussin, R.S.Al-Hasnawy, R.I.Jasim, N.F.Habubi, S.S.Chiad, J.Green.Eng. 10, 701, 2020.

[104] Y.Larbah,M. Adnane,B.Rahal, Semico-nductors.54, 1439, 2020.

[105] D. P. Volanti, D. Keyson, L.S. Cavalcante, A.Z. Sim oes, M.R. Joya, E.Longo, J. A. Varela, P. S. Pizani, A. G. Souza, J. Alloys Compd. 459, 2008.

[106] K. A. Kazem, A. A. Habib, K. M. Abdul Latif, Effect of irradiation on electronic transfer film CuO by chemical pyrolysis deposition, Journal of Diala, 36, 2009.

[107] B. K. Mohammed and M. A. Hassan, Study of Some Structural, Optical Properties of Copper Oxide Thin Films Deposited by Chemical Spray Pyrolysis Method, Journal of Engineering and Technology, 29, 15, 635-649, 2011.

[108] S. Roy, A. H. Bhuiyan, Properties of Spray Pyrolysied Copper Oxide Thin Films, Sensors and Transducers, Vol. 209, Issue 2, pp 20-27, 2017.

[109] A. F. Khan, M. Mehmoud, A. M. Rana. M. T. Bhatti, A. Mahmood, Phys.Lett 7, 2009.

[110] V. Anand, A. Sakthivelu, K. Deva Arun Kumar, S. Valanarasu, A. Kathalingam et al, Ceram.Int.44, 6730, 2018.

[111] T.Z.Khodair, H.A.Adwan, H.N.Shallal, diyala J. Pure Sci13,198, 2017.

[112] J. Morales, L. Sanchez, F. Martin, J. R. Ramos-Barrado, M. Sanchez, Use of low-temperature nanostructured CuO thin films deposited by spraypyrolysis in lithium cells, Thin Solid Films, 474,pp. 133– 140, 2005.

[113] Papadimitropoulos G., Vourdas N, Vamvakas V. E.and Davazoglou D, Deposition and characterization of copper oxide thin films, J. Phys: Conf. Ser, 10, pp. 182–185, 2005.

[114] Marabelli F., Parraviciny G. B, Orioli F. S, Optical gap of CuO, Phys. Rev. B., 52, pp 1433–1436, 2005.

[115] S. Roy, A. H. Bhuiyan, Properties of Spray Pyrolysied Copper Oxide Thin Films, Sensors and Transducers, Vol. 209, Issue 2, pp 20-27, 2017.

[116] A. Alkaya, R. Kaplan, H. Canbolat, S.S. Hegedus, A comparaison of fill factor and recombination losses in amorphous silicon solar cells on ZnO and SnO2, Renewable energy, 34, 1595-1599, 2009.

[117] A. F. Khan, M. Mehmoud, A. M. Rana. M. T. Bhatti, A. Mahmood, Phys.Lett 7, 2009.

[118] R. D.Prabu, S. Valanarasu, H. A. H. Geno, A. Jegatha Christy, K.Jeyadheepan et al, J.Mater. Sci.Mater Electron.29 10921, 2018.

[119] Y.S. Yu, G.Y. Kim, B.H. Min, S.C. Kim, J. Eur. Ceram. Soc. 24, 1865, 2004.

[120] J.I. Pankove, Optical Processes in Semiconductors, second ed., Courier DoverPublication Inc., New York, NY, 2010.

[121] V. Anand, A. Sakthivelu, K. Deva Arun Kumar, S. Valanarasu, A. Kathalingam et al, Ceram.Int.44, 6730, 2018.

الجمهورية الجزائرية الديمقراطية الشعبية
République Algérienne Démocratique et Populaire
وزارة التعليـــــــــم العالـــــــــي و البحث العلمـــــــي
Ministère de l'Enseignement Supérieur et de la Recherche Scientifique

Université 20 Août 1955 - Skikda
Faculté des Sciences
Bibliothéque de la faculté

جـامعة 20 أوت 1955- سكيكدة
كـــــلية العلـــــوم
مكتبـة الكليـة

سكيكدة في 11/ 07/2024

بطاقة معلومات خاصة بمذكرة التخرج

اسم و لقب الطالب : رقم التسجيل :

* بودفح أسماء * 36019321 *
* * *
* * *
* * *

اسم و لقب المشرف على المذكرة : Daira Radouane

عنوان المذكرة : Structural, optical and electrical characterisation of Li-doped CuO thin layers obtained by spray pyrolysis.

القسم : الفيزياء

المستوى : ماستر

التخصص : فيزياء اشعاعية

الجمهورية الجزائرية الديمقراطية الشعبية

Ministère de l'enseignement supérieur et la recherche scientifique
Université Du 20 Aout 1955-SKIKDA-
Faculté des Sciences
DEPARTEMENT de physique

وزارة التعليم العالي و البحث العلمي
جامعة20أوت 1955سكيكدة-
كلية العلوم
قسم الفيزياء

N°...../ D. A /2024

رقم :...../ ق ع ف / 2024

Skikda le :

Autorisation de dépôt de Mémoire de Master

Je soussigné : ...Daira Radouane.....

Certifie que l'étudiant (e) :.....Boudefaa asma.....

.....

.....

.....

Spécialité :.....physique des rayonnements.....

Intitulé :.....Etude structurale, optique et électriques des.....

.....couches minces de CuO dopées Li obtenues.....

.....par spray pyrolyse.....

A apporté les corrections relatives à son travail de mémoire de master.

Visa de l'encadrant